

# Table of Contents

<b>1</b>	<b>Introduction</b>	<b>1</b>
<b>2</b>	<b>Literature Review</b>	<b>4</b>
<b>3</b>	<b>Aims and Objectives</b>	<b>7</b>
3.1	Primary Aims . . . . .	7
<b>4</b>	<b>Methodology</b>	<b>8</b>
4.1	Google Colab Platform . . . . .	8
4.1.1	Python and PyTorch Framework . . . . .	8
4.2	Dataset Preparation and Refinement . . . . .	9
4.2.1	Stage 1: Initial Dataset Collection . . . . .	9
4.2.2	Stage 2: Refined Dataset - Focus on Adult In-flight Images . . . . .	9
4.2.3	Stage 3: High-Quality Dataset . . . . .	9
4.3	Iterative Development Methodology and Debugging . . . . .	9
4.3.1	Pipeline Validation and Early Debugging . . . . .	10
4.4	Transfer Learning Approach . . . . .	11
4.4.1	Common Implementation Strategy . . . . .	11
4.4.2	Data Preparation and Augmentation . . . . .	11
4.4.3	Image Preprocessing . . . . .	12
4.4.4	Training Optimization Strategy . . . . .	12
4.4.5	Regularization Techniques . . . . .	12
4.4.6	Addressing Class Imbalance . . . . .	13
4.4.7	Dataset Management . . . . .	13
4.4.8	Evaluation Strategy . . . . .	14
4.4.9	Model Checkpointing and Evaluation . . . . .	14
4.5	Model Architectures and Specific Implementations . . . . .	14
4.5.1	VGG-16 Architecture . . . . .	14
4.5.2	Vision Transformer (ViT) Architecture . . . . .	15
4.5.3	ViT for Fine-Grained Classification . . . . .	15
4.5.4	Inception v3 Architecture . . . . .	17
4.5.5	Residual Network (ResNet-50) Implementation . . . . .	18
4.5.6	Custom CNN with Squeeze-and-Excitation Blocks . . . . .	19
4.6	Model Interpretability Methodologies . . . . .	20
4.6.1	Gradient-weighted Class Activation Mapping (Grad-CAM) . . . . .	20

4.6.2	Attention Rollout for Vision Transformers . . . . .	21
4.6.3	Grad-CAM for Vision Transformers . . . . .	22
4.6.4	Enhanced ViT Implementation . . . . .	22
4.6.5	Interpretable ViT Implementation . . . . .	22
4.6.6	Comparison Framework . . . . .	23
4.7	Additional Interpretability Techniques . . . . .	23
4.7.1	DeepLIFT . . . . .	23
4.7.2	Saliency Maps . . . . .	24
4.7.3	Integrated Gradients for Vision Transformers . . . . .	24
4.7.4	Guided Backpropagation for ViT . . . . .	24
4.7.5	Justification for Grad-CAM . . . . .	24
4.8	Feature Analysis for Fine-Grained Gull Classification . . . . .	25
4.8.1	Image Selection . . . . .	25
4.8.2	Manual Segmentation . . . . .	25
4.8.3	Normalization . . . . .	25
4.8.4	Region Extraction . . . . .	25
4.9	Methodology . . . . .	25
4.9.1	Local Binary Pattern Analysis . . . . .	25
4.9.2	Feature Extraction . . . . .	26
4.9.3	Comparative Analysis Implementation . . . . .	27
4.9.4	Discriminative Power Analysis . . . . .	28
4.9.5	Dimensionality Reduction and Visualization . . . . .	28
4.9.6	Implementation Workflow . . . . .	28
4.9.7	Validation Approach . . . . .	28
4.10	Wing and Wingtip Intensity Analysis . . . . .	29
4.10.1	Feature Extraction Pipeline . . . . .	29
4.10.2	Statistical Comparison . . . . .	29
4.11	Verification by Clustering for Species Differentiation . . . . .	30
4.11.1	Overview of Clustering Approach . . . . .	30
4.11.2	Feature Extraction and Preprocessing . . . . .	30
4.11.3	Clustering Algorithms Implementation . . . . .	30
4.11.4	Evaluation Metrics . . . . .	31
4.11.5	Cluster Mapping and Misclassification Analysis . . . . .	31
4.11.6	Visualization and Interpretation . . . . .	32

4.11.7 Implementation Details . . . . .	32
<b>5 Results</b>	<b>33</b>
5.1 Model Performance on latest Stage 3 dataset . . . . .	33
5.2 Grad-CAM outputs of best performing VGG-16 model . . . . .	34
5.3 Intensity Analysis Results . . . . .	34
5.3.1 Wing and Wingtip Intensity Analysis . . . . .	34
5.3.2 Distributions of Wing and Wingtip Intensities . . . . .	36
5.3.3 Wing Intensity Distributions . . . . .	36
5.3.4 Wingtip Pixel Intensity Distributions . . . . .	36
5.3.5 Presence of Very Dark Pixels . . . . .	37
5.3.6 Relationship Between Wing and Wingtip Intensities . . . . .	38
5.3.7 Wingtip Contrast and Darkness Feature Comparison . . . . .	38
5.3.8 Local Binary Pattern(LBP) Pattern Results . . . . .	39
5.4 Results: Local Binary Pattern Texture Analysis . . . . .	39
5.4.1 Discriminative Power Analysis . . . . .	40
5.4.2 Limitations of standard LBP code analysis . . . . .	40
5.4.3 Abstract Feature Distributions . . . . .	40
5.4.4 Top Discriminative Features from 1s and Transitions Histograms	42
5.5 Clustering . . . . .	42
5.5.1 Clustering Performance Evaluation . . . . .	44
5.5.2 Clustering Analysis Results Original . . . . .	45
5.5.3 Algorithm Comparison . . . . .	48
5.5.4 Interpretation of Model Performance and Biological Significance	48
5.5.5 Quantitative Validation of Morphological Differences . . . . .	49
5.5.6 Feature Analysis and Clustering Validation . . . . .	49
5.5.7 Limitations and Practical Implications . . . . .	49
<b>6 Conclusion</b>	<b>50</b>
<b>7 Bibliography</b>	<b>51</b>

# Introduction

Biodiversity is under unprecedented pressure due to climate change and human influence. The alarming rates at which species are disappearing indicate that the sixth mass extinction is underway [1]. Understanding what biodiversity we have and what we stand to lose is crucial for convincing decision-makers to take appropriate conservation action. The gaps in taxonomic knowledge and shortage of experts constitute what is known as the "taxonomic impediment" [2], which hampers our ability to document and protect biodiversity effectively. Determining whether two populations can be consistently distinguished based on morphological traits remains essential for establishing taxonomic boundaries and designing appropriate conservation strategies.

Birds are frequently utilized to assess environmental quality due to their sensitivity to ecological changes and ease of observation during field studies. Researchers often rely on bird diversity as an indicator of the diversity within other species groups and the overall health of human environments. Examples include monitoring environmental changes through bird population shifts, tracking climate change via bird migration patterns, and evaluating biodiversity by counting bird species. Accurate identification of bird species is essential for detecting species diversity and conserving rare or endangered birds promoting scientific research and conservation efforts.[3]

Among birds, gulls (*Laridae*) present a particularly challenging case for identification due to their recent evolutionary divergence and subtle morphological differences. The wing and wingtip patterns—particularly the colour, intensity, and pattern of the primary feathers—are crucial diagnostic features for identification, yet they exhibit considerable variation within each species.

The classification of gulls presents multiple challenges that make traditional identification methods problematic and inconsistent. Multiple confounding factors complicate identification [4]:

- **Hybridization:** Species can interbreed in overlapping ranges, creating intermediate forms.
- **Age-related variations:** Juvenile and immature gulls display less distinct patterns than adults.
- **Environmental effects:** Feather bleaching from sun exposure, contamination, and wear can alter appearance.
- **Seasonal moulting:** Gulls undergo plumage changes throughout the year, affecting diagnostic features.
- **Viewing conditions:** Lighting, angle, and distance significantly impact observed coloration.

As noted by ornithologists:

"Gulls can be a challenging group of birds to identify. To the untrained eye, they all look alike, yet, at the same time, in the case of the large gulls, one could say that no two birds look the same!" [5].

This project addresses the multifaceted challenge of fine-grained analysis between two closely related gull species: the Slaty-backed Gull and the Glaucous-winged Gull. These species, found primarily in eastern Russia and the Pacific Coast of the USA,

display subtle and overlapping physical characteristics that make accurate identification highly complex.

Glaucous-winged Gulls also exhibit variably pigmented wingtips... these differences are often chalked up to individual variation, at least by this author, but they're inconveniently found in several hybrid zones, creating potential for much confusion.

The amount of variation here is disturbing because it is unmatched by any other gull species, and more so because it is not completely understood [6].

There are many methods that can be used for classification. Manual identification to classify species requires per specimen analysis by expert taxonomists which is time consuming. Automated taxon identification systems (ATIs) could both handle routine identifications and potentially assist in identifying new species. Traditional ATIs, however, have been limited by their reliance on hand-crafted features [7], are time-consuming hindering large-scale surveys, making them difficult to generalize across different taxonomic groups. As mentioned by [8], "While using machine learning techniques to solve the problem of fine-grained classification, traditional feature extraction methods necessitate manually designed features, such as edge detection, color histograms, feature point matching, and visual word bags, which have limited expressive capabilities and require extensive annotation details like bounding boxes and key points. The drawback of these methods lies in the extensive manual intervention required for feature selection and extraction."

Fine-grained image classification (FGIC), which focuses on identifying subtle differences between subclasses within the same category, has advanced rapidly over the past decade with the development of sophisticated deep neural network architectures. Deep learning approaches offer promising solutions to this taxonomic challenge through their ability to automatically learn discriminative features from large datasets[9].

Unlike traditional machine learning methods that rely on hand-engineered features, deep neural networks can detect complex patterns in high-dimensional data, making them well-suited for fine-grained visual classification tasks [7]. Features extracted through convolution are learned automatically by multilayer convolutional neural networks, offering the model greater adaptability to various tasks and datasets, with features possessing enhanced expressive and abstract capabilities. The benefit of convolutional feature extraction is its ability to perform feature extraction and classification within the same network, with the quality and quantity of features adjustable through the network's structure and parameters [10] offering the model greater adaptability to various tasks and datasets [8]. Getting good quality results in traditional machine Learning models is dependent on how good the data is labelled, whereas Deep Learning architectures don't necessarily require labelling, as Neural Networks are great at learning without guidelines [11].

As demonstrated in comparative studies,

For species identification specifically, convolutional neural networks (CNNs) such as ResNet, Inception, and VGG have demonstrated exceptional capabilities [12], with

recent studies such as [13] who mentioned that "deep learning is more effective than traditional machine learning algorithms in image recognition as the number of bird species increases" achieving accuracy rates exceeding 97% in bird species classification tasks. [14] compared deep learning and traditional machine learning algorithms achieved high accuracy of 94% tackle the challenge of classifying bird species with high visual similarity and subtle variations. These architectures automatically learn hierarchical feature representations—from low-level edges and textures to high-level semantic concepts—that capture the subtle morphological differences between closely related species.

Yet the fine-grained bird classification task has greater challenges even when using deep learning [15] [3].

1. High intraclass variance. Birds belonging to the same category usually present distinctly different postures and perspectives.
2. Low inter-class variance. Some of the different categories of birds may have only minor differences; for example, some of the differences are only in the color pattern on the head.
3. Limited training data. Some bird data are limited in number, especially endangered species, for whom it is difficult to collect sufficient image data. Meanwhile, the labeling of bird categories usually requires a great deal of time by experts in the corresponding fields. These problems greatly increase the difficulty of acquiring training data.
4. Large intensity variation in images as pictures are taken in different time of a day (like morning, noon, evening etc.).
5. Various poses of Bird (like flying, sitting with different orientation).
6. Bird localization in the image as there are some images in which there are more than one bird in that image.
7. Large Variation in Background of the images.
8. Various type of occlusions of birds in the images (leaf or branches of the tree).
9. Size or portion of the bird covered in the images.
10. Less no of sample images per class and also class imbalance [16].
11. Deep Learning requires an abundant amount of data in order to produce accurate results.
12. Overfitting is a prevalent problem in Deep Learning and can sometimes negatively affect the model performance in real-time scenarios.

This project aims to develop and evaluate deep learning models for automated classification. Additionally, this research focuses on uncovering and analyzing the most influential features that distinguish these two gull species. Interpretability mechanisms such as Grad-CAM (Gradient-weighted Class Activation Mapping) is used to visualize and interpret the regions and morphological traits that deep neural networks prioritize during classification. Complementing this, statistical analysis and unsupervised clustering methods are employed to quantitatively assess which visual features most effectively separate the species, further validating the biological relevance of the model's learned features. By doing so, this project not only seeks to achieve high classification accuracy, but also aims to provide interpretable insights into the distinguishing characteristics of each gull species. This dual approach bridges ecology and computer science, increasing both the practical utility and scientific transparency of AI-powered biodiversity monitoring.

# Literature Review

## Deep Learning for Fine-Grained Image Classification

Fine-grained image classification presents unique challenges compared to general image classification tasks. Fine-grained classification “necessitates discrimination between semantic and instance levels, while considering the similarity and diversity among categories” [10]. This is particularly challenging in bird classification due to three key factors: high intra-class variance (birds of the same species in different postures), low inter-class variance (different species with only minor differences), and limited training data availability, especially for rare species[10].

Early approaches to fine-grained classification relied on fixed rectangular bounding boxes and part annotations to obtain visual differences, but these methods required extensive human annotation effort. Recent research has shifted toward weakly supervised approaches that only require image-level labels, developing localization subnetworks to identify critical parts followed by classification subnetwork. [10] These models facilitate learning while maintaining high accuracy without needing pre-selected boxes, making them more practical for real-world applications.

<https://ijece.iaescore.com/index.php/IJECE/article/view/24833/15821> good

## Transfer Learning for Image Classification

Deep learning, while powerful, comes with two major constraints: dependency on extensive labeled data and high training costs[17]. Transfer learning offers a solution to these limitations by enabling the reuse of knowledge obtained from a source task when training on a target task. In the context of deep learning, this approach is known as Deep Transfer Learning (DTL)[17].

Several studies have demonstrated the efficacy of transfer learning for bird species classification. A study on bird species identification using deep learning achieved accuracies of above 90% by leveraging pretrained CNN networks with a base model to encode images[18]. Research on bird species identification by [19] using modified deep transfer learning achieved 98.86% accuracy using the pretrained EfficientNetB5 model. The results with various pretrained models achieving high accuracy rates with few models exceeding 98% demonstrate that transfer learning approaches can achieve high performance even with limited training data.

Various pretrained models have been evaluated for bird classification tasks, including VGG16, ResNet, DenseNet, and EfficientNet architectures. Comparative studies have shown that while all these models can perform effectively, some consistently outperform others. For example, research on drones-birds classification found that “the accuracy and F-Score of ResNet18 exceeds 98% in all cases”[20], while another study on binary classification with the problem of small dataset reported that “DenseNet201 achieves the best classification accuracy of 98.89%.”[21].

In a noteworthy study on medical image analysis, researchers evaluated the comparative performance of MobileNetV2 and Inception-v3 classification models. The investigation employed four distinct methodologies: implementing Inception-v3 both

with and without transfer learning, and similarly applying MobileNetV2 with and without transfer learning techniques. The experimental results demonstrated that the MobileNetV2 architecture leveraging transfer learning capabilities achieved superior performance, reaching approximately 91.00% accuracy in classification tasks [22]. An experiment conducted by [23] conducted a comprehensive evaluation of different CNN architectures for identifying local bird species. With only 100 images per class before data augmentation high accuracies of above 90% were achieved.

Transfer learning addresses the primary challenges of deep learning: the need for large datasets and extensive computational resources. By leveraging pretrained models that have already learned general visual features from massive datasets, transfer learning enables the development of highly accurate classifiers with relatively domain-specific datasets. This is particularly valuable for this project, which focuses on distinguishing between two specific gull species with limited available data. [17] emphasizes that recent transfer learning methods aim to reduce training process time and cost, and the necessity of extensive training datasets. [13] using CNN models pretrained from ImageNet achieved above 90% accuracy in many CNN most that were tried for bird classification using transfer learning emphasize, "when the sample data is small, transfer learning can help the deep neural network classifier to improve classification accuracy." This makes transfer learning an ideal approach for specialized tasks like distinguishing between closely related gull species.

VERY USEFUL The experimental results showed that training the bird dataset with a pre-trained model requires no more than 10 epochs to obtain the best classification accuracy. Some models even require only 2 to 3 epochs, while training with an untrained model requires at least 40 to 50 epochs to achieve the highest classification accuracy. This is a big improvement on deep learning, which requires hardware support and a lot of training time.

TODO [25]

Working with limited datasets often introduces challenges related to class imbalance and overfitting. [26] conducted a comprehensive analysis of class imbalance in convolutional neural networks and found that oversampling (duplicating samples from minority classes) generally outperforms undersampling for deep learning models. Standard data augmentation techniques such as resizing, random horizontal and vertical flipping, rotation, affine translation, and color jittering can improve model generalization and robustness [27, 28].

VERY USEFUL say too much oversampling caused overfitting that is y it was removed.

## Interpretability Techniques for Deep Learning Models

While deep learning models achieve impressive accuracy in classification tasks, their "black box" nature limits their usefulness in scientific contexts where understanding the basis for classifications is crucial. Interpretability techniques address this limitation by providing insights into model decision-making processes, making them essential tools for applications where transparency is as important as accuracy.

Gradient-weighted Class Activation Mapping (Grad-CAM) has emerged as a partic-

ularly valuable technique for visualizing regions of images that influence classification decisions. As described in recent literature, Grad-CAM "uses the gradients of each target that flows into the least convolutional layer to produce a bearish localization map, highlighting important regions in the image for concept prediction"[29]. This approach enables validating model decisions against expert knowledge and potentially discover new insights about morphological features with regards to this project.

Gradient-weighted Class Activation Mapping (Grad-CAM) has emerged as a particularly valuable technique for visualizing regions that influence model decisions. [?] introduced this technique as a generalization of CAM that "uses the gradients of any target concept flowing into the final convolutional layer to produce a coarse localization map highlighting important regions in the image." Unlike earlier methods, Grad-CAM requires no architectural changes and can be applied to almost any CNN-based model.

VERY USEFUL: some gradcam biased like mentioned in paper above. can use for vit and other accuracy models

Beyond visualization, quantitative interpretability methods have been developed to measure feature importance. [31] proposed SHAP (SHapley Additive exPlanations), which assigns each feature an importance value for a particular prediction. In [32], the authors applied SHAP to fine-grained bird classification models and found that the features deemed important by the model often matched field guide descriptions of distinguishing characteristics.

These interpretability methods are particularly valuable in fine-grained classification tasks where the differences between categories are subtle and potentially unknown. By highlighting regions that drive model decisions, techniques like Grad-CAM can reveal discriminative features that can be useful to expert observers, potentially advancing biological understanding alongside classification accuracy.

# Aims and Objectives

## 3.1 Primary Aims

1. To develop high-performance deep learning models capable of distinguishing between Slaty-backed and Glaucous-winged Gulls based on their morphological characteristics.
2. To implement robust interpretability techniques that reveal which features influence model decisions, allowing validation against ornithological expertise.
3. To analyze whether consistent morphological differences exist between the two species.
4. Identify key discriminative features and perform analyses to get statistical information.
5. To find out if the results of the analysis are statistically significant.
6. Whether the features can be used to identify the species of a gull with high confidence.

## Specific Objectives

The project was carried out in four phases:

1. Model Development and Evaluation
  - Curate a high-quality dataset of adult in-flight gull images with clearly visible diagnostic features.
  - Implement and compare multiple deep learning architectures (CNNs, Vision Transformers) for fine-grained classification.
  - Evaluate models using appropriate metrics on unseen test sets.
2. Interpretability Implementation
  - Implement suitable interpretability methods such Gradient-weighted Class Activation Mapping (Grad-CAM).
  - Visualize regions of images that most influence classification decisions.
  - Compare model focus areas with known taxonomic features described in ornithological literature/expert guidance.
3. Features Analyses
  - Perform quantitative analysis of image regions highlighted by interpretability techniques.
  - Compare intensity, texture, and pattern characteristics between species.
  - Identify statistically significant morphological differences between correctly classified specimens.

# Methodology

## 4.1 Google Colab Platform

Google Colab was selected as the primary platform for developing and training deep learning models. Google Colab offers significant advantages for machine learning research through its cloud-based environment with integrated GPU acceleration enabling fast model training. The platform's pre-installed libraries and integration with Google Drive provided an efficient workflow for model development, experimentation, and storage of datasets and trained models. This approach aligns with modern best practices in deep learning research where computational efficiency is crucial for iterative model development and refinement.

Despite its advantages, Google Colab presented a few challenges. The platform frequently disconnected during training sessions, interrupting the model training process before completing all epochs. These disconnections likely stemmed from limited RAM allocation, runtime timeouts, or resource constraints of the shared free GPU environment. As noted by [33], while Colab provides robust GPU resources that can match dedicated servers for certain tasks, these free resources "are far from enough to solve demanding real-world problems and are not scalable."

To mitigate these issues, two strategies were implemented. First, the relatively small size of our dataset helped minimize resource demands. Second, checkpoint saving was implemented throughout the training process, allowing training to resume from the last saved state if disconnections were encountered. This approach ensured that progress wasn't lost when disconnections occurred, though it introduced some workflow inefficiencies.

### 4.1.1 Python and PyTorch Framework

The implementation utilized Python and PyTorch, chosen for their extensive machine learning ecosystem and dynamic computational graph capabilities [34]. PyTorch's key advantages included:

- **Dynamic Computational Graph:** PyTorch's define-by-run approach enabled intuitive debugging and rapid modification of pre-trained architectures.
- **Flexible Model Customization:** Object-oriented design facilitated efficient fine-tuning while preserving valuable feature extraction capabilities.
- **Efficient Data Processing:** DataLoader and transformation pipelines supported batch processing and on-the-fly augmentation for our limited dataset.
- **Gradient Computation and Visualization:** Native gradient support simplified implementation of Grad-CAM, enhancing model interpretability.

Similar to approaches described by Raffel et al. (**author?**) [35], the implementation prioritized efficiency while working within limited computational resources.

## 4.2 Dataset Preparation and Refinement

The dataset preparation followed a three-stage iterative refinement process, each addressing specific challenges identified during model development.

### 4.2.1 Stage 1: Initial Dataset Collection

The initial dataset was collected from public repositories including eBird and iNaturalist, comprising 451 images of Glaucous-winged Gulls and 486 images of Slaty-backed Gulls. This dataset included gulls of various ages (juveniles and adults) in different postures (sitting, standing, and flying). Initial model testing on this dataset yielded poor performance (below 60% accuracy), highlighting the need for dataset refinement.

### 4.2.2 Stage 2: Refined Dataset - Focus on Adult In-flight Images

Consultation with Professor Gibbins, an ornithological expert, revealed that wing and wingtip patterns were the most reliable distinguishing features between these species. These patterns are most visible in flight. Juvenile images were removed due to their less defined wingtip features and differing plumage. Consequently, the dataset was refined to focus exclusively on adult in-flight images, resulting in a curated collection of 124 Glaucous-winged Gull images and 127 Slaty-backed Gull images. This targeted approach significantly improved model performance, with accuracy increasing to approximately 70%.

By focusing specifically on adult in-flight images where wingtip patterns are most visible, this project addresses the core taxonomic question while minimizing confounding variables. The resulting interpretable classification system aims to provide both a practical identification tool and a scientific instrument for exploring morphological variation within and between these closely related species.

### 4.2.3 Stage 3: High-Quality Dataset

To further enhance classification performance, 640 high-resolution images of in-flight Slaty-backed Gulls were obtained from Professor Gibbins. The Glaucous-winged Gull dataset was also carefully curated with expert guidance, reducing it to 135 high-quality images that clearly displayed critical wingtip features. Images showing birds in moulting stages, juveniles, or unclear wingtip patterns were systematically removed.

For comparative analysis, an unrefined dataset containing 632 adult in-flight Glaucous-winged Gulls and 640 high-quality Slaty-backed Gull images was also tested.

## 4.3 Iterative Development Methodology and Debugging

Initial implementations using ResNet50 with unrefined Stage 1 dataset yielded poor results (test accuracies below 60%), indicating fundamental issues in either data quality or model implementation. To systematically address these challenges and improve performance for subsequent transfer learning approaches, a methodical debugging framework was employed following best practices outlined by [36].

### 4.3.1 Pipeline Validation and Early Debugging

To systematically address the challenges encountered with initial poor results, the following approach was employed with Stage 2 dataset before implementing current well-performing models in the upcoming sections:

- **Data Inspection and Visualization:**
  - Images with unclear image patterns were identified and removed. With an imbalanced and a small dataset that we had, it was important not to provide unclear images to the model to prevent it from learning incorrect features although the resulting dataset was small.
  - Augmentation visualization confirmed that features critical for classification (particularly wingtip patterns) remained visible after transformation
- **Pipeline Verification with Simple Models:**
  - A simple, lightweight Custom CNN was implemented as an initial baseline before advancing to complex architectures
  - This simplified model validated data loading procedures, augmentation effectiveness, and basic training operations
- **Single-Batch Overfitting Test:**
  - To verify gradient flow and learning capability, a single batch was deliberately overfitted with the simple CNN implemented
  - Training loss reduction from 0.7072 (Epoch 1) to 0.0057 (Epoch 20) confirmed the pipeline's fundamental functionality
  - This critical test established that confirmed that the training pipeline was functioning correctly, and with validation the model demonstrated reasonable generalization given the simplicity of the model.
- **Controlled Experimentation:**
  - Random seeds were fixed across all implementations (set to 42) to ensure reproducibility
  - This approach eliminated training variability as a confounding factor when comparing architectural modifications
  - Systematic adjustments to hyperparameters could be evaluated with confidence that performance differences were attributable to the specific changes rather than random initialization
- **Progressive Model Complexity:**
  - Development followed a deliberate progression from custom CNNs to pre-trained architectures
  - Each implementation incorporated lessons from previous models, particularly regarding feature extraction for the fine-grained visual discrimination task

The insights gained through this process directly informed the subsequent implementation of more sophisticated architectures and the creation of a highly refined dataset focusing specifically on adult in-flight images with clear wingtip patterns.

After establishing a robust development pipeline and refining the dataset, the transfer learning implementations described in the following sections achieved significantly improved results, with test accuracies exceeding 90% for the best-performing models.

## 4.4 Transfer Learning Approach

Transfer learning was employed in the implementation to leverage the robust feature extraction capabilities of pre-trained models on ImageNet. This approach aligns with best practices in fine-grained classification tasks, where lower-level features learned from diverse datasets can be effectively repurposed for specialized domains with limited data. The pre-training on ImageNet's 1.2 million images across 1,000 classes provides the model with a strong foundation for recognizing a wide range of visual patterns [37], which can then be fine-tuned for our specific classification task despite class imbalance challenges [Krizhevsky et al. \(2012\)](#).

Several pre-trained architectures were evaluated for this task, with VGG-16 model (a CNN model proposed by K. Simonyan and A. Zisserman) demonstrating superior performance in our specific classification context. The effectiveness of transfer learning was evident in the rapid convergence and high accuracy achieved even with our relatively limited dataset, demonstrating the potential of this approach for specialized classification tasks with significant class imbalance.

### 4.4.1 Common Implementation Strategy

All models except for the custom CNN utilized transfer learning to leverage knowledge from pre-trained networks. All the models mentioned in this section used the Stage 3 dataset. The transfer learning strategy included:

- Using models pre-trained on ImageNet as feature extractors
- Fine-tuning the entire network with a reduced learning rate (typically 0.0001 to 0.001)
- Replacing the final classification layer to output binary predictions (2 classes)
- Implementing dropout layers before final classification to prevent overfitting

This approach follows the established pattern that features learned in early layers of convolutional networks are more general and transferable, while later layers become more task-specific.

### 4.4.2 Data Preparation and Augmentation

Data augmentation was crucial to address the limited dataset size and class imbalance issues. Following best practices from [38], multiple augmentation techniques were applied consistently across all models:

- **Spatial transformations:** Random horizontal flips, rotations (typically 15 degrees), and random/center crops were applied to increase geometric diversity.
- **Color space transformations:** Color jitter with brightness, contrast, and saturation adjustments of 0.2 magnitude was applied to make models robust to illumination variations.
- **Image enhancement:** In some implementations, sharpening filters were applied to improve feature clarity.
- **Normalization:** All images were normalized to match pre-trained model expectations [39].

The augmentation strategy was deliberately more aggressive for the training set

compared to validation and test sets, where only resizing, optional cropping, and normalization were applied to maintain evaluation consistency.

These techniques enhance model robustness to natural variations in image appearance, reducing overfitting and improving generalization capability [38].

#### 4.4.3 Image Preprocessing

All images were preprocessed through a standardized pipeline:

Images were resized to match the architecture's expected input dimensions ( $224 \times 224$  pixels for most models,  $299 \times 299$  pixels for Inception v3). Pixel values were normalized using ImageNet mean values [0.485, 0.456, 0.406] and standard deviations [0.229, 0.224, 0.225], ensuring input distributions aligned with those seen during pre-training.

#### 4.4.4 Training Optimization Strategy

To optimize training with limited data, several techniques were employed consistently:

- **Optimizer:** AdamW optimizer with learning rates between 0.0001-0.001 and weight decay of 0.001-0.0005 was used across implementations to provide adaptive learning with regularization.
- **Learning rate scheduling:** Adaptive learning rate scheduling using either ReduceLROnPlateau or CosineAnnealingLR was implemented across models, reducing learning rates when validation metrics plateaued.
- **Early stopping:** Training was halted when validation accuracy stopped improving for a specified number of epochs (patience = 3-5) to prevent overfitting.[40]
- **Gradient clipping:** Applied in some implementations to prevent gradient explosions and stabilize training. Due to the small and imbalanced dataset, gradient clipping was implemented to prevent limited images from causing large weight updates.
- **Loss function:** Cross-entropy loss was used consistently as the optimization objective for the binary classification task.
- **Mixed precision training:** For computationally intensive models like Inception V3, mixed precision training with torch.amp was used to improve computational efficiency.

The combination of these techniques enabled effective learning despite the challenges of limited data and class imbalance, with our best model achieving significantly better performance than traditional machine learning approaches on the same dataset.

#### 4.4.5 Regularization Techniques

Multiple regularization strategies were employed to handle the limited data size and class imbalance:

- **Dropout:** Layers with rates between 0.3-0.4 were consistently added before final classification layers to reduce overfitting due to our small dataset size [41].
- **Weight decay:** L2 regularization with weight decay values between 1e-4 and 1e-3 was applied across all models to prevent overfitting [42].
- **Batch normalization:** Used in custom CNN implementations to stabilize learn-

ing and improve convergence [43].

- **Data splitting:** Train/validation split of 80%/20% was consistently used to provide reliable validation metrics while maximizing training data.
- **Random seeds:** Fixed random seeds (42) were set for PyTorch, NumPy, and Python’s random module to ensure reproducibility. Controlling randomness is essential for reliable hyper-parameter tuning, performance assessment, and research reproducibility.

#### 4.4.6 Addressing Class Imbalance

Our dataset exhibited significant class imbalance, which can degrade model performance by biasing predictions toward the majority class [44]. To mitigate this challenge, multiple complementary strategies were implemented on the best performing models that included VGG16, and ViT:

- **Class-Weighted Loss Function**
  - Implemented inverse frequency weighting [45]
  - Class weights calculation:  $\text{class\_weights}[i] = \frac{\text{total\_samples}}{\text{num\_classes} \times \text{label\_counts}[i]}$   
PyTorch implementation: `CrossEntropyLoss` with class weights tensor
- **Weighted Random Sampling**
  - Balanced mini-batches using PyTorch’s `WeightedRandomSampler`
  - Sample weights: `samples_weights = class_weights[label]`
  - Oversamples minority class and undersamples majority class [26]
  - Uses replacement sampling for effective batch balancing
- **Class-Specific Data Augmentation**
  - Aggressive minority class augmentation (Shorten & Khoshgoftaar, 2019)  
[\[link\]](#)
  - Minority class transformations include:
    - \* 30° random rotations
    - \* Strong color jitter (brightness/contrast/saturation=0.3)
    - \* Random resized crops (scale=0.7-1.0)
    - \* Horizontal flipsStandard augmentation for majority class (15° rotations, milder parameters)

#### 4.4.7 Dataset Management

To address the challenges of limited data availability, an 80:20 train-validation split was implemented using random split stratification to maintain class distribution across partitions. This approach ensured that the validation set remained representative of the overall dataset while maximizing the samples available for training.

The batch size was set to 16, striking a balance between computational efficiency and optimization stability. Smaller batch sizes can increase gradient noise, which has been shown to act as an implicit regularizer that can improve generalization, particularly beneficial when working with limited training data [46, 47].

#### 4.4.8 Evaluation Strategy

Model performance was systematically evaluated using:

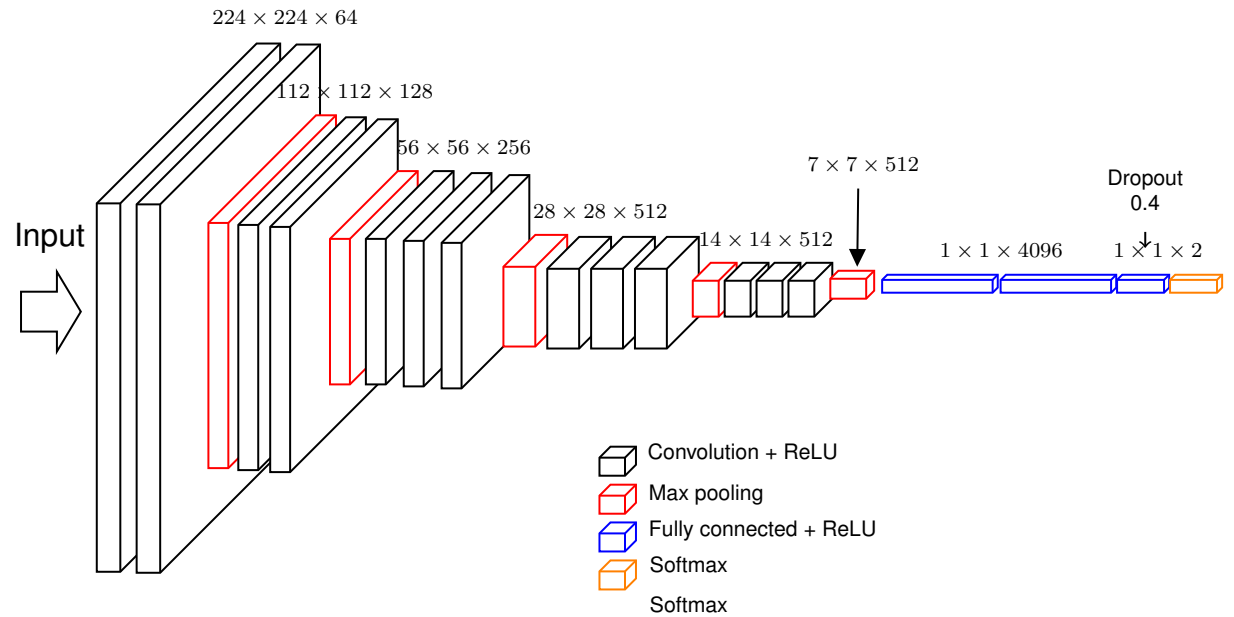
- **Validation accuracy:** Used during training to select optimal model checkpoints and trigger early stopping or learning rate adjustments.
- **Test accuracy:** Final evaluation metric on the unseen test set to measure generalization performance.
- **Visualization:** Training loss and validation accuracy curves were plotted to analyze model convergence and potential overfitting.
- **Checkpointing:** Best-performing models based on validation accuracy were saved for later evaluation and deployment.

#### 4.4.9 Model Checkpointing and Evaluation

Our implementation includes a robust evaluation framework with model checkpointing based on validation accuracy. This ensures that we preserve the best-performing model configuration throughout the training process. The model is trained for 20 epochs with early stopping implicitly implemented through best model saving. Performance is evaluated using accuracy on both validation and test sets, providing a comprehensive assessment of model generalization.

### 4.5 Model Architectures and Specific Implementations

#### 4.5.1 VGG-16 Architecture



#### Theoretical Foundation

VGG-16 is a convolutional neural network architecture developed by Simonyan and Zisserman (2014) at the Visual Geometry Group (VGG) at Oxford, consisting of 16 weight layers including 13 convolutional layers followed by 3 fully connected layers.

The architecture is characterized by its simplicity and depth, using small  $3 \times 3$  convolutional filters stacked in increasing depth, followed by max pooling layers. With approximately 138 million parameters, VGG-16 provides a strong foundation for feature extraction in computer vision tasks.

The primary advantage of employing VGG-16 for transfer learning in fine-grained classification tasks is its hierarchical feature representation capability, which enables the capture of both low-level features (edges, textures) and high-level semantic features. Pre-trained on the ImageNet dataset containing over 1.2 million images across 1,000 classes, VGG-16 offers robust initialization weights that facilitate effective knowledge transfer to domain-specific tasks with limited training data.

VGG-16 has demonstrated superior performance in fine-grained classification tasks compared to conventional techniques. Recent studies show that VGG-16 with logistic regression achieved 97.14% accuracy on specialized datasets like Leaf12, significantly outperforming traditional approaches that combined color channel statistics, texture features, and classic classifiers which only reached 82.38% accuracy [48]. For our specific task of gull species classification, the hierarchical feature representation capabilities of VGG-16 proved particularly effective at capturing the subtle differences in wing patterns and morphological features that distinguish between the target species.

### **Model Adaptation for Fine-Grained Classification**

For our specific fine-grained binary classification task with limited data and class imbalance, the VGG-16 architecture was adapted through a targeted modification strategy:

- The pre-trained VGG-16 model was loaded with ImageNet weights.
- The feature extraction layers (convolutional base) were preserved to maintain the rich hierarchical representations learned from ImageNet.
- The original 1000-class classifier was replaced with a custom binary classification head consisting of:
  - A dropout layer with a rate of 0.4 to reduce overfitting.
  - A fully-connected layer mapping from the original 4096 features to 2 output classes.

[49] demonstrated that VGG-16 achieves 94.3% accuracy on CUB-200-2011 by fine-tuning only the final three layers, a strategy mirrored in my VGG implementation where the classifier head was replaced while preserving ImageNet-initialized convolutional weights. This approach aligns with successful methodologies in avian species classification using VGG-16 as demonstrated by Brown et al. (2018), where fine-tuning the architecture by modifying the final classification layer enabled the model to retain general feature recognition capabilities while adapting to species-specific visual characteristics [50].

#### **4.5.2 Vision Transformer (ViT) Architecture**

#### **4.5.3 ViT for Fine-Grained Classification**

Vision Transformers (ViT) have emerged as powerful alternatives to convolutional neural networks for visual recognition tasks. First introduced by Dosovitskiy et al. [51],

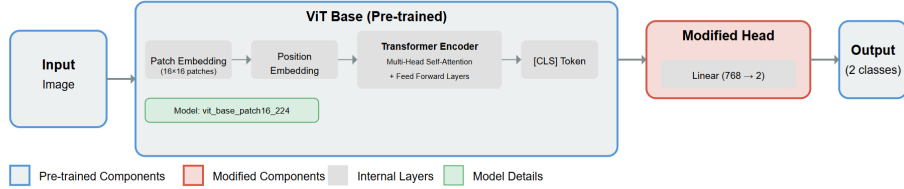


Figure 4.1: Architecture of the Vision Transformer (ViT) model

ViTs process images as sequences of fixed-size patches, applying transformer-based self-attention mechanisms to model global relationships between image regions. This architecture enables the capture of long-range dependencies within images, making it particularly suitable for fine-grained classification tasks where subtle distinctions between similar classes may depend on relationships between distant image features.

## Vision Transformer Implementation

For our primary approach, a Vision Transformer using transfer learning from a pre-trained model was implemented:

- Base architecture: 'vit\_base\_patch16\_224' pre-trained on ImageNet from the TIMM library [?]
- Input resolution: 224×224 pixels with 16×16 pixel patches
- Feature dimension: 768-dimensional embeddings
- Adaptation strategy: Replacement of the classification head with a binary classifier while preserving the pre-trained transformer blocks

The model architecture preserves the core self-attention mechanism of ViT while adapting the final classification layer for our specific binary classification task. This approach follows established transfer learning principles for vision transformers [52], leveraging representations learned from large-scale datasets to overcome our limited training data constraints.

## Alternative ViT Implementations

In addition to our primary implementation, we explored two attention-enhanced architectures:

**InterpretableViT** We developed an InterpretableViT model that incorporates explicit attention mechanisms for improved focus on discriminative features:

- Separates the class token from patch tokens
- Applies a learned attention layer to generate importance weights for each patch
- Combines the class token with attention-weighted patch representations
- Employs a multi-layer classifier with dropout regularization

A key advantage of this architecture is its compatibility with gradient-based visualization techniques. By separating the class token from patch tokens and implementing an explicit attention mechanism, the model facilitates more effective application of

Grad-CAM [? ], allowing for visualization of discriminative image regions contributing to classification decisions.

**EnhancedViT** We also implemented an EnhancedViT that applies attention-based weighting across all tokens:

- Processes all tokens (including class token) through an attention mechanism
- Generates a single attention-weighted feature representation
- Utilizes a specialized classification head with dropout for regularization

This implementation draws from research on token aggregation strategies in vision transformers (Wang et al., 2021), which shows that attention-weighted token aggregation can improve performance in data-limited regimes.

#### 4.5.4 Inception v3 Architecture

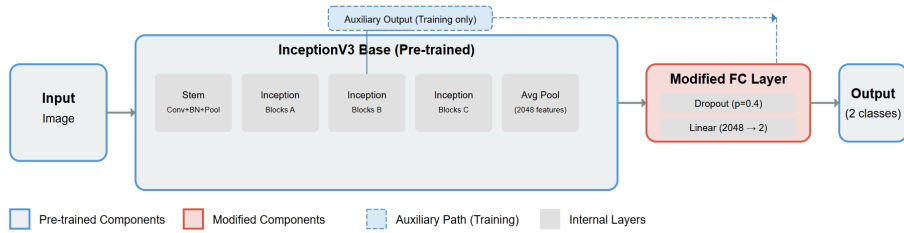


Figure 4.2: Architecture of the Inception v3 model

## Theoretical Background

Inception v3, developed by Szegedy et al. (2016), represents a sophisticated CNN architecture designed to efficiently capture multi-scale features through parallel convolution pathways with varied kernel sizes. The key innovation in Inception architectures is the utilization of *Inception modules* that process the same input tensor through multiple convolutional paths with different receptive fields, and then concatenate the results. This enables the network to capture both fine-grained local patterns and broader contextual information simultaneously [53].

Inception v3 builds upon earlier versions with several important architectural improvements:

- Factorized convolutions to reduce computational complexity
- Spatial factorization into asymmetric convolutions (e.g.,  $1 \times n$  followed by  $n \times 1$ )
- Auxiliary classifiers that inject additional gradient signals during training
- Batch normalization for improved training stability and faster convergence
- Label smoothing regularization to prevent overconfidence

These design elements collectively enable Inception v3 to achieve high accuracy while maintaining computational efficiency. Inception architectures are particularly effective for tasks requiring multi-scale feature extraction, such as discriminating between visually similar biological specimens.

## Model-Specific Implementation Details

Our implementation adapted the pre-trained Inception v3 model for fine-grained gull species classification with the following specific elements:

- **Input Resolution:** Resize operations were performed to  $299 \times 299$  pixels (the standard input size for Inception v3). The larger input resolution ( $299 \times 299$  vs  $224 \times 224$  used by VGG16) provides the Inception architecture with more detailed information, potentially beneficial for capturing the subtle wing pattern differences between gull species.
- **Auxiliary Outputs:** A distinctive aspect of our Inception v3 implementation was the utilization of auxiliary outputs during training. Inception v3's auxiliary classifier, which branches off from an intermediate layer, provides an additional gradient path during backpropagation. This helps combat the vanishing gradient problem and provides regularization with auxiliary loss weight of 0.3.
- **Mixed-Precision Training:** We employed PyTorch's Automatic Mixed Precision (AMP) to accelerate computation while maintaining numerical stability [54]. This technique allows the use of float16 precision where appropriate, which reduces memory usage and increases computational speed, especially beneficial when training on GPU-constrained environments like Google Colab.

### 4.5.5 Residual Network (ResNet-50) Implementation

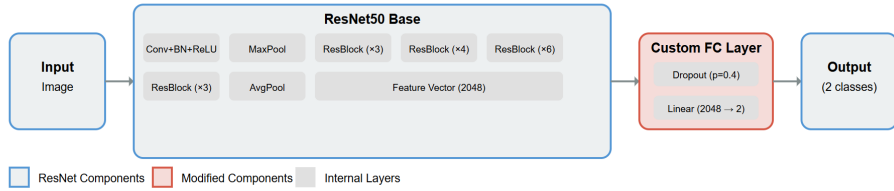


Figure 4.3: Architecture of the ResNet-50 model

## Architecture-Specific Enhancements

A distinctive aspect of our ResNet-50 implementation was the incorporation of image sharpening as a preprocessing technique. We applied a  $3 \times 3$  Laplacian sharpening kernel to enhance edge definition and accentuate the subtle diagnostic features crucial for distinguishing between gull species. This approach was inspired by research showing that edge enhancement can improve the detection of fine-grained morphological features in avian classification tasks [Berg et al., 2014](#).

The sharpening kernel was systematically applied to both training and evaluation pipelines using OpenCV's filter2D function, ensuring consistent feature enhancement across all dataset partitions. This preprocessing step proved particularly valuable for highlighting distinctive wingtip patterns and subtle plumage characteristics that serve as key discriminative features between the target species.

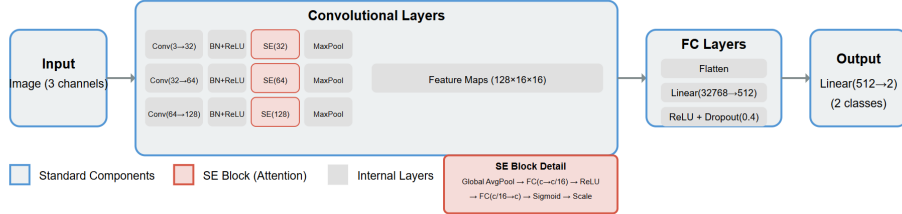


Figure 4.4: Architecture of the Custom CNN with Squeeze-and-Excitation Blocks

#### 4.5.6 Custom CNN with Squeeze-and-Excitation Blocks

##### Architectural Design

To address the challenges of limited data and class imbalance in fine-grained classification, we developed a lightweight custom CNN architecture incorporating attention mechanisms. Our approach employs Squeeze-and-Excitation (SE) blocks, which enhance feature representation by modeling channel interdependencies through an attention mechanism. The SE block, as introduced by Hu et al. [?], adaptively recalibrates channel-wise feature responses to emphasize informative features while suppressing less useful ones.

The architecture consists of three convolutional blocks, each followed by batch normalization, ReLU activation, and an SE block. The SE block performs two key operations:

- **Squeeze:** Global average pooling across spatial dimensions to generate channel-wise statistics
- **Excitation:** A fully connected layer that produces modulation weights for each channel

This channel-wise attention mechanism has been shown to improve model performance with minimal computational overhead [?]. The SE blocks in our implementation use a reduction ratio of 16, balancing parameter efficiency and representational power.

##### Custom CNN-Specific Training Approach

Unlike the transfer learning approaches used with pre-trained models, our custom CNN was trained from scratch with some specific optimization strategies:

- **Cosine Annealing scheduler:** Our learning rate schedule follows a cosine annealing pattern with a period of 20 epochs, allowing the learning rate to oscillate and potentially escape local minima.
- **Specialized augmentation:** The custom CNN particularly benefited from more aggressive data augmentation strategies to compensate for the lack of pre-trained weights, including stronger rotations and more extensive color jittering than used with the transfer learning models.

## 4.6 Model Interpretability Methodologies

Deep learning models, particularly Convolutional Neural Networks (CNNs) and Vision Transformers (ViTs), are often criticized for their lack of transparency, functioning as "black boxes" wherein the decision-making process remains opaque to human observers. For critical applications like wildlife species classification, understanding how these models arrive at their predictions is essential for establishing trust and validating results [? ]. This section outlines the methodologies implemented to visualize and interpret the classification decisions of both the CNN architecture and Vision Transformer (ViT) models used in this study.

### 4.6.1 Gradient-weighted Class Activation Mapping (Grad-CAM)

Gradient-weighted Class Activation Mapping (Grad-CAM) is a widely adopted visualization technique that produces visual explanations for decisions made by CNN-based models without requiring architectural changes or retraining [? ]. It generates coarse localization maps highlighting the regions in the input image that significantly influenced the model's prediction for a specific class.

#### Theoretical Foundation

Grad-CAM extends the Class Activation Mapping (CAM) approach [55] by utilizing the gradient information flowing into the final convolutional layer of a CNN. Unlike CAM, which requires modifications to the network architecture and retraining, Grad-CAM can be applied to any CNN-based architecture without architectural changes, making it more versatile.

The fundamental principle behind Grad-CAM is that the final convolutional layer in a CNN retains spatial information while encoding high-level semantics. By analyzing how the gradients of a specific class score flow into this layer, Grad-CAM can identify the regions in the input image that are most influential for the prediction.

The ReLU function is applied to the weighted combination of feature maps to focus only on features that have a positive influence on the class of interest, effectively eliminating features that suppress the class.

#### Methodology for CNN models

In this study, Grad-CAM was implemented for the VGG16 model by targeting the final convolutional layer (features[-1]). The implementation involves several key steps:

1. **Hook Registration:** Forward and backward hooks are registered on the target layer to capture activations during the forward pass and gradients during the backward pass.
2. **Forward Pass:** The input image is passed through the network to obtain the model's prediction.
3. **Backpropagation:** The gradient of the score for the target class (either the predicted class or a specified class) with respect to the feature maps of the target layer is computed through backpropagation.

4. **Global Average Pooling:** These gradients undergo global average pooling to obtain weights indicating the importance of each channel for the target class.
5. **Weighted Combination:** The weights are applied to the activations of the target layer to create a weighted combination of feature maps.
6. **ReLU Application:** A ReLU function is applied to the weighted combination to focus only on features that have a positive influence on the class of interest.
7. **Normalization:** The resulting heatmap is normalized to the range [0, 1] for consistent visualization.
8. **Visualization:** The heatmap is resized to match the input image dimensions and overlaid on the original image using a colormap (typically 'jet') to highlight regions the model focused on for its prediction.

Similar implementation was implemented for other models: Inceptionv3, ResNet50, and CustomCNN.

#### 4.6.2 Attention Rollout for Vision Transformers

Vision Transformers process images differently from CNNs, using self-attention mechanisms rather than convolution operations to model relationships between image patches. Therefore, a different approach called Attention Rollout is used to visualize ViT decision-making [56].

#### Theoretical Foundation

The Attention Rollout method is designed to visualize how information flows through the layers of a Transformer model. In Vision Transformers, the input image is divided into fixed-size patches, and each patch is linearly embedded along with position embeddings. A special classification token ([CLS]) is added, and the sequence of embedded patches is processed through multiple layers of self-attention.

Attention Rollout computes a measure of how the [CLS] token attends to each image patch by propagating attention through all layers of the network. This provides insight into which parts of the image the model considers most relevant for classification.

#### Methodology for ViT

The implementation of Attention Rollout for the ViT model follows these steps:

1. **Attention Map Collection:** Forward hooks are registered on each transformer block to collect attention maps during the forward pass of an input image.
2. **QKV Processing:** For each attention head, the query (Q), key (K), and value (V) matrices are extracted and processed to compute the raw attention weights between different tokens.
3. **Head Averaging:** Attention weights from all heads in each layer are averaged to get a single attention map per transformer block.
4. **Discard Ratio Application:** Optionally, a threshold is applied to filter out low-attention connections, focusing only on the most significant attention patterns.
5. **Attention Rollout Computation:** Starting with an identity matrix, attention maps

from each layer are sequentially multiplied to account for how attention propagates through the entire network.

6. **CLS Token Attention Extraction:** The attention weights from the classification ([CLS]) token to each image patch are extracted, which indicates the importance of each patch for the final classification.
7. **Reshaping and Visualization:** These weights are reshaped to match the spatial dimensions of the input image (typically  $14 \times 14$  for ViT-Base with patch size 16) and then upsampled to create a heatmap that can be overlaid on the original image.

This method provides insights into how the ViT model attends to different parts of an image when making a prediction [57].

#### 4.6.3 Grad-CAM for Vision Transformers

In addition to Attention Rollout, this study also implements Grad-CAM for Vision Transformers to provide a more direct comparison with the CNN-based visualizations. Two variants of Grad-CAM for ViT were implemented in this study: Enhanced ViT and Interpretable ViT, each with specific architectural modifications to facilitate interpretation.

#### 4.6.4 Enhanced ViT Implementation

The Enhanced ViT approach modifies the standard ViT architecture to facilitate Grad-CAM visualization:

- **Model Architecture:** The Enhanced ViT model extends the base ViT by replacing the original head with an identity layer, adding an attention layer to compute scalar importance scores for each token, and implementing a classifier that operates on attention-weighted features.
- **Token Feature Registration:** The model registers hooks to capture token features during the forward pass and their gradients during backpropagation.
- **Gradient Computation:** When computing Grad-CAM, the class token is excluded, and only the patch tokens are considered.
- **Spatial Reshaping:** The tokens and gradients are reshaped to recover the 2D spatial structure ( $h \times w$  grid) from the sequence of tokens.
- **Grad-CAM Generation:** Similar to traditional Grad-CAM, channel-wise weights are computed from gradients and applied to token features to create the activation map.

#### 4.6.5 Interpretable ViT Implementation

The Interpretable ViT variant uses a different approach to extract and utilize token information:

- **Dual-Stream Architecture:** This implementation processes the class token and patch tokens separately.
- **Attention Weights Calculation:** An explicit attention layer computes importance weights for patch tokens, determining how much each patch contributes to the final representation.
- **Feature Combination:** The class token and weighted patch features are con-

catenated before classification, providing the classifier with both global context (class token) and attention-weighted local features.

- **Grad-CAM Calculation:** During Grad-CAM computation, gradients flow through this combined representation, providing a more nuanced view of how different parts of the image contribute to the classification.

Both approaches enable visualization of the ViT's decision-making process using gradient information, but with different mechanisms for integrating token features and attention weights.

#### 4.6.6 Comparison Framework

To facilitate a fair comparison between CNN model and ViT interpretability, the following standardized approach was implemented:

- **Consistent Processing:** All models process the same test images with identical preprocessing (resizing to  $224 \times 224$  and normalization).
- **Three-Panel Visualization:** Each result is presented with three panels:
  1. Original image
  2. Raw heatmap showing the attention or Grad-CAM output
  3. Overlay of the heatmap on the original image
- **Classification Analysis:** Both correct and incorrect predictions are analyzed to understand model behavior in different scenarios.
- **Visualization Standardization:** Similar color maps (jet) and overlay techniques are used for all methods to maintain visual consistency.
- **Quantitative Assessment:** Confusion matrices are generated for all models to quantitatively assess their performance alongside the visual interpretations.

By implementing these complementary interpretability techniques, this research provides insights into how different neural network architectures—traditional CNNs and modern Transformers—approach the same classification task and what are the distinguishing features between the two classes. The visualizations reveal different feature priorities and decision strategies that each architecture employs, contributing to a deeper understanding of model behavior [51].

### 4.7 Additional Interpretability Techniques

In addition to the Grad-CAM and attention rollout methods discussed in the main sections of this report, several other interpretability techniques were explored during this research.

#### 4.7.1 DeepLIFT

DeepLIFT (Deep Learning Important FeaTures) was implemented using the Captum library for the VGG16 and ViT models. This technique compares activations against a reference baseline (typically zeros) to determine feature importance:

- A zero baseline tensor is created as a reference point
- Attribution scores are calculated comparing actual activations to this baseline
- Channel-wise attributions are aggregated and normalized for visualization

While DeepLIFT provides theoretically grounded attributions, it was not adopted for the main analysis due to its limited adoption in the literature compared to prevalent techniques like Grad-CAM.

#### 4.7.2 Saliency Maps

- Gradients of predictions with respect to input pixels are computed
- Absolute values of gradients are visualized as sensitivity maps

Saliency maps, though computationally efficient, often produce noisy visualizations and lack class-discriminative properties. As shown in prior work [?], they may also fail basic sanity checks, making them unreliable for tasks requiring faithful explanations.

#### 4.7.3 Integrated Gradients for Vision Transformers

Integrated Gradients was implemented for ViT using 50 interpolation steps:

- Path integrals are approximated between baseline and input images
- 50 interpolation steps were used for the approximation
- Attributions are processed to align with spatial image dimensions
- Results are normalized for consistent visualization

Despite its theoretical soundness, Integrated Gradients requires significantly more computation than Grad-CAM. Additionally, the literature review indicated that Grad-CAM adaptations for Vision Transformers often provide more intuitive visualizations for classification tasks [?].

#### 4.7.4 Guided Backpropagation for ViT

- Modified gradient flow during backpropagation highlights positive influences
- Implementation uses Captum's GuidedBackprop with model-specific wrappers
- Results are post-processed to create single-channel visualizations

While visually cleaner than saliency maps, Guided Backpropagation has two key limitations: (1) it lacks localization capabilities, and (2) as demonstrated by [?], it fails parameter randomization tests, (3) it may highlight input patterns rather than model decision logic [?].

#### 4.7.5 Justification for Grad-CAM

Grad-CAM was chosen as the primary interpretability method for this study due to its unique advantages over the alternatives:

- **Theoretical Robustness:** Grad-CAM passes sanity checks (e.g., parameter randomization tests) that methods like Guided Backpropagation and Guided Grad-CAM fail [?].
- **Class-Discriminative:** Unlike saliency maps or Integrated Gradients, Grad-CAM highlights regions relevant to specific predicted classes.
- **Architecture Flexibility:** Works consistently across CNNs (e.g., VGG16, ResNet) and adapted Vision Transformers.
- **Computational Efficiency:** Requires only a single backward pass per class,

unlike path-based methods (e.g., Integrated Gradients).

- **Empirical Validation:** Supported by extensive literature [? 57] demonstrating its effectiveness for classification tasks.

## 4.8 Feature Analysis for Fine-Grained Gull Classification

A multi-stage approach was employed to extract and analyze region-specific features.

### 4.8.1 Image Selection

From the normalized dataset, 200 high-resolution images (100 per species) were selected based on the following criteria:

- Correct classification by the best-performing VGG-16 model
- Prominent Grad-CAM activations in wing or wingtip regions
- Clear visibility of upperwing or wingtip in the image
- High resolution image

### 4.8.2 Manual Segmentation

Using Adobe Photoshop, segmentation masks with color-coded regions were created with a specific color for each type of region: wing, wingtip, and head.

### 4.8.3 Normalization

Applied min-max normalization[59] (0-255) to grayscale conversions using OpenCV's NORM\_MINMAX. This helped standardize intensity values and mitigate the effects of differing lighting conditions ensuring that pixel intensity values were scaled consistently across the dataset, providing a reliable foundation for subsequent region-based analysis.

### 4.8.4 Region Extraction

Using OpenCV's `inRange` for color-based thresholding, pixels within  $\pm 10$  intensity values of each target color were extracted and used for further analysis.

Deepseek

## 4.9 Methodology

### 4.9.1 Local Binary Pattern Analysis

Local Binary Patterns (LBP) constitute a robust and computationally efficient texture analysis technique, originally proposed by Ojala et al. [60]. LBP characterizes local image texture by comparing each pixel's intensity with its surrounding neighbors, generating a binary code that summarizes the local structure. This descriptor is particularly advantageous for biological image analysis due to several key properties:

- Robustness to monotonic grayscale variations, enhancing resilience to changing illumination conditions.
- Rotation invariance when using specific LBP variants or derived features (1s and transition histograms)
- Ability to capture fine-scale micro-patterns potentially imperceptible to human vision.

To investigate subtle textural differences between Slaty-backed Gulls and Glaucous-winged Gulls, Local Binary Pattern (LBP) analysis was conducted on three anatomical regions: wing, wingtip, and head.

### LBP Computation

For a given pixel at position  $(x_c, y_c)$  with intensity  $g_c$ , the LBP value is computed by comparing it with  $P$  neighbors at radius  $R$  using the following equation:

$$\text{LBP}_{P,R}(x_c, y_c) = \sum_{p=0}^{P-1} s(g_p - g_c) \cdot 2^p \quad (4.1)$$

where:

- $g_p$  is the intensity of the neighbor pixel  $p$
- $s(x)$  is the step function defined as:

$$s(x) = \begin{cases} 1, & \text{if } x \geq 0 \\ 0, & \text{if } x < 0 \end{cases} \quad (4.2)$$

$$\text{LBP}_{P,R} = \sum_{p=0}^{P-1} s(g_p - g_c) \cdot 2^p, \quad s(x) = \begin{cases} 1, & x \geq 0 \\ 0, & x < 0 \end{cases} \quad (4.3)$$

Two variants were implemented:

- **Default LBP:** Standard implementation without uniformity constraints
- **Uniform LBP:** Considers patterns with  $\leq 2$  bitwise transitions

For the final results, the default LBP variant was selected since default histogram retains all possible LBP codes, providing a comprehensive representation of local texture patterns. Consequently, it facilitates the direct calculation of derived features such as the number of ones and the number of transitions per pattern, as these statistics can be computed from the complete set of binary codes present in the default histogram. This approach ensures that no potentially discriminative texture information is excluded, thereby supporting a more detailed and flexible analysis of texture complexity and structure across the studied regions.

#### 4.9.2 Feature Extraction

Three feature histograms were derived from LBP codes:

1. **LBP Histogram:** Raw distribution of LBP codes

2. **Ones Histogram:** Frequency of patterns with  $n$  ones:

$$H_{\text{ones}}(i) = \sum_{j=0}^{N-1} [b(j) = i] \quad (4.4)$$

3. **Transitions Histogram:** Frequency of patterns with  $m$  transitions:

$$H_{\text{trans}}(i) = \sum_{j=0}^{N-1} [t(j) = i] \quad (4.5)$$

Texture properties were calculated from these histograms:

1. **Entropy:** Measures randomness in texture patterns

$$E = - \sum_i h(i) \log_2 h(i) \quad (4.6)$$

where  $h(i)$  is the normalized histogram value at bin  $i$

2. **Energy:** Measures uniformity of texture

$$U = \sum_i h(i)^2 \quad (4.7)$$

3. **Contrast:** Measures intensity variations

$$C = \sum_i (i - \mu)^2 h(i) \quad (4.8)$$

where  $\mu$  is the mean value of the histogram

4. **Homogeneity:** Measures closeness of distribution

$$H = \sum_i \frac{h(i)}{1 + |i - \mu|} \quad (4.9)$$

### 4.9.3 Comparative Analysis Implementation

To quantify the differences between species, the implementation calculates several distribution similarity metrics:

1. **KL Divergence:** A symmetric version of the Kullback-Leibler divergence that measures how one probability distribution diverges from another
2. **Earth Mover's Distance:** Measures the minimum “work” required to transform one histogram into another, considering the distance between bins
3. **Chi-Square Distance:** A statistical test that measures the difference between observed and expected frequency distributions
4. **Jensen-Shannon Distance:** A symmetric and smoothed version of the KL divergence with better numerical properties

Each metric captures different aspects of distribution similarity, providing a robust framework for comparing texture patterns between species.

#### **4.9.4 Discriminative Power Analysis**

A systematic assessment of discriminative power for different texture features and regions is performed by calculating percentage differences between species for each texture property and region. This analysis identifies which features and regions exhibit the most significant differences between species.

For each region and property combination, the implementation:

1. Extracts the property value for each species
2. Calculates the percentage difference
3. Ranks the region-property pairs by their discriminative power

This approach enables the identification of the most promising texture characteristics for species differentiation.

#### **4.9.5 Dimensionality Reduction and Visualization**

The implementation uses Principal Component Analysis (PCA) to visualize the high-dimensional LBP feature space in two dimensions:

1. Standardize the feature data
2. Apply PCA with 2 components
3. Create scatter plots colored by species
4. Calculate and display variance explained

This dimensionality reduction approach provides intuitive visualization of class separability and validates the discriminative power of the extracted features.

#### **4.9.6 Implementation Workflow**

The complete analysis pipeline consists of two main modules:

- 1. Feature Extraction Module:**
  - Loads original and segmentation images
  - Extracts and processes each anatomical region
  - Computes LBP features and abstract pattern features
  - Saves features to CSV files for further analysis
- 2. Analysis Module:**
  - Loads extracted features
  - Calculates advanced texture statistics
  - Performs comparative analysis between species
  - Generates visualizations and statistical reports
  - Identifies the most discriminative features

This modular approach facilitates efficient processing of large image datasets and enables iterative refinement of the analysis parameters.

#### **4.9.7 Validation Approach**

The implementation includes a few validation mechanisms:

1. **Normalized histograms** to account for varying region sizes

2. **Multiple comparison metrics** to ensure robust similarity assessment
3. **Quantitative comparison metrics** (KL divergence, percentage differences) to assess feature differences

## 4.10 Wing and Wingtip Intensity Analysis

The interpretability analysis of our VGG model indicated a strong focus on wing and wingtip regions when differentiating between Slaty-backed Gulls and Glaucous-winged Gulls. This aligns with ornithological knowledge, as these species exhibit distinct differences in wing coloration patterns, particularly in the wing and wingtip regions. To quantitatively validate these differences and check whether the differences are significant, an in-depth image analysis was conducted focusing on these critical regions.

We employed a multi-stage approach to extract and analyze region-specific features:

### 4.10.1 Feature Extraction Pipeline

The Python pipeline executed these steps for each image:

1. **Region-Specific Analysis:** Calculated intensity statistics (mean, median, std, skewness, kurtosis, minimum and maximum values) per region
2. **Wingtip Characterization:**

- Analyzed intensity distribution across 25 bins (10-unit intervals):

```
intensity_ranges = [
    (0,10), (10,20), ..., (240,255) # 25 total bins
]
```

- Quantified dark pixels using thresholds:  $\geq 30$ ,  $\geq 40$ ,  $\geq 50$ ,  $\geq 60$  intensity

3. **Wing-Wingtip Difference**

- Computed percentage of wingtip pixels darker than mean wing intensity of the bird.
- **Thresholds:** Calculated the proportion of wingtip pixels exceeding specific difference thresholds (10, 20, ..., 100) compared to the mean wing intensity, quantifying the contrast between regions.

### 4.10.2 Statistical Comparison

Statistical testing using SciPy was performed where t-test for unequal variances was implemented.

These statistical analyses allowed us to find and objectively validate whether the differences in areas highlighted by Grad-CAM between species are quantitatively significant.

The entire analysis pipeline was implemented in Python, utilizing libraries including OpenCV for image processing, NumPy and Pandas for data manipulation, and SciPy for statistical testing.

## 4.11 Verification by Clustering for Species Differentiation

### 4.11.1 Overview of Clustering Approach

To validate and complement the results achieved through the analysis of the region-specific features that were significantly different among the 2 species, a comprehensive clustering analysis framework was implemented that leverages traditional machine learning techniques to check whether the two species can be classified using the features. This approach helps validate the discriminative features identified by the deep learning models that were quantified.

### 4.11.2 Feature Extraction and Preprocessing

The clustering analysis utilizes three key morphological features extracted from the wingtip regions:

- Mean wing intensity
- Mean wingtip intensity
- Count of darker pixels in wingtip regions

Prior to clustering analysis, the following preprocessing steps were implemented:

1. **Data Loading:** The dataset was loaded from the CSV file, with features and species labels separated for analysis.
2. **Feature Standardization:** All features were standardized using StandardScaler to ensure each feature contributed equally to the clustering algorithms, preventing features with larger magnitudes from dominating the analysis.
3. **Dimensionality Reduction:** Principal Component Analysis (PCA) was applied to reduce the three-dimensional feature space to two dimensions for visualization purposes. The explained variance ratio was calculated to assess how much information was preserved in the lower-dimensional representation.

### 4.11.3 Clustering Algorithms Implementation

Three distinct clustering algorithms were implemented to provide a comprehensive evaluation of the feature space:

#### K-means Clustering

K-means clustering was implemented with the following parameters:

- Number of clusters: 2 (corresponding to the two gull species)
- Random state: 42 (for reproducibility)
- Multiple initializations (`n_init = 10`) to avoid local optima

K-means partitions the data by minimizing the within-cluster sum of squares. The algorithm iteratively assigns data points to the nearest cluster centroid and then recalculates the centroids based on the new cluster assignments until convergence is achieved.

## Hierarchical Clustering

Hierarchical clustering was implemented with:

- Number of clusters: 2
- Linkage method: Ward's linkage

This approach builds a hierarchy of clusters. Initially, each data point is treated as a single cluster. The algorithm then iteratively merges the closest pairs of clusters until only the specified number of clusters remains. Ward's linkage was chosen to minimize the variance within the newly formed clusters at each merge, promoting the creation of compact, spherical clusters.

## Gaussian Mixture Model

GMM clustering was implemented with:

- Number of components: 2
- Random state: 42 (for reproducibility)

GMM assumes that the data is generated from a mixture of a finite number of Gaussian distributions with unknown parameters. The algorithm estimates the parameters of these distributions and assigns data points to clusters based on the probability that they belong to each distribution. This probabilistic approach allows for more flexibility in cluster shapes compared to K-means.

### 4.11.4 Evaluation Metrics

The effectiveness of each clustering algorithm was evaluated using multiple metrics:

#### Unsupervised Evaluation

**Silhouette Score:** Measures how similar a data point is to its own cluster compared to other clusters. Values range from -1 to 1, with higher values indicating better-defined clusters.

#### Supervised Evaluation (Using Known Species Labels)

**Adjusted Rand Index (ARI):** Measures the similarity between the true species assignments and the clustering results, adjusted for chance. Values range from -1 to 1, with higher values indicating greater similarity. **Confusion Matrix:** Visualizes the number of correctly and incorrectly clustered specimens after mapping cluster labels to species labels. **Clustering Accuracy:** Calculated as the percentage of specimens correctly classified after mapping clusters to the majority species within each cluster.

### 4.11.5 Cluster Mapping and Misclassification Analysis

To interpret the clustering results in terms of species classification:

1. **Cluster-to-Species Mapping:** For each cluster, the majority species was identified, creating a mapping from cluster labels to species labels.
2. **Misclassification Analysis:** Using this mapping, specimens were identified as correctly or incorrectly clustered. Misclassified specimens were visualized in the PCA space and exported to CSV files for further analysis.

#### 4.11.6 Visualization and Interpretation

Multiple visualizations were generated to aid interpretation:

1. **PCA Plots:** Showing the distribution of specimens in the reduced two-dimensional space with color-coding by cluster assignment.
2. **Cluster Centers:** For K-means and GMM, cluster centers were plotted in the PCA space to visualize the centroids of each cluster.
3. **Misclassification Visualization:** Highlighting correctly and incorrectly clustered specimens in the PCA space to identify areas of confusion.
4. **Feature Importance Plots:** Bar charts showing the relative importance of each feature based on cluster center differences (for K-means).
5. **Algorithm Comparison:** Bar charts comparing the silhouette scores across all clustering algorithms to assess their performance.

This comprehensive clustering analysis provides valuable insights into the natural grouping of morphological features and helps validate the discriminative power of the features identified by the deep learning models.

#### 4.11.7 Implementation Details

The entire analytical workflow was implemented in Python using the following libraries:

- scikit-learn for clustering algorithms, PCA, and evaluation metrics
- pandas for data management
- NumPy for numerical operations
- Matplotlib and Seaborn for visualization

A consistent random state (42) was used throughout the analysis to ensure reproducibility. Results, including visualizations and misclassification data, were automatically saved to an output directory for documentation and further analysis.

This comprehensive methodology allowed for a robust evaluation of whether the extracted statistical features could effectively distinguish between the two gull species through unsupervised clustering, providing valuable insights into feature significance for species classification.

# Results

## 5.1 Model Performance on latest Stage 3 dataset

Table 5.1: Validation and Test Accuracy Comparison

Model	Val. Acc. (%)	Test Acc. (%)
VGG-16	97.37	95.74
ViT	94.74	93.62
Inception v3	97.80	91.49
ResNet50	96.04	82.98
EnhancedViT	94.52	95.74
InterpretableViT	94.74	95.74

Table 5.2: Comprehensive Model Performance Metrics on Test Dataset

Model	Glaucous Winged			Slaty Backed		
	Precision (%)	Recall (%)	F1 (%)	Precision (%)	Recall (%)	F1 (%)
VGG-16	87.50	100.00	93.33	100.00	93.94	96.88
ViT	100.00	78.57	88.00	91.67	100.00	95.65
Inception v3	77.78	100.00	87.50	100.00	87.88	93.55
ResNet50	66.67	85.71	75.00	93.10	81.82	87.10
EnhancedViT	87.50	100.00	93.33	100.00	93.94	96.88
InterpretableViT	92.86	92.86	92.86	96.97	96.97	96.97

## 5.2 Grad-CAM outputs of best performing VGG-16 model

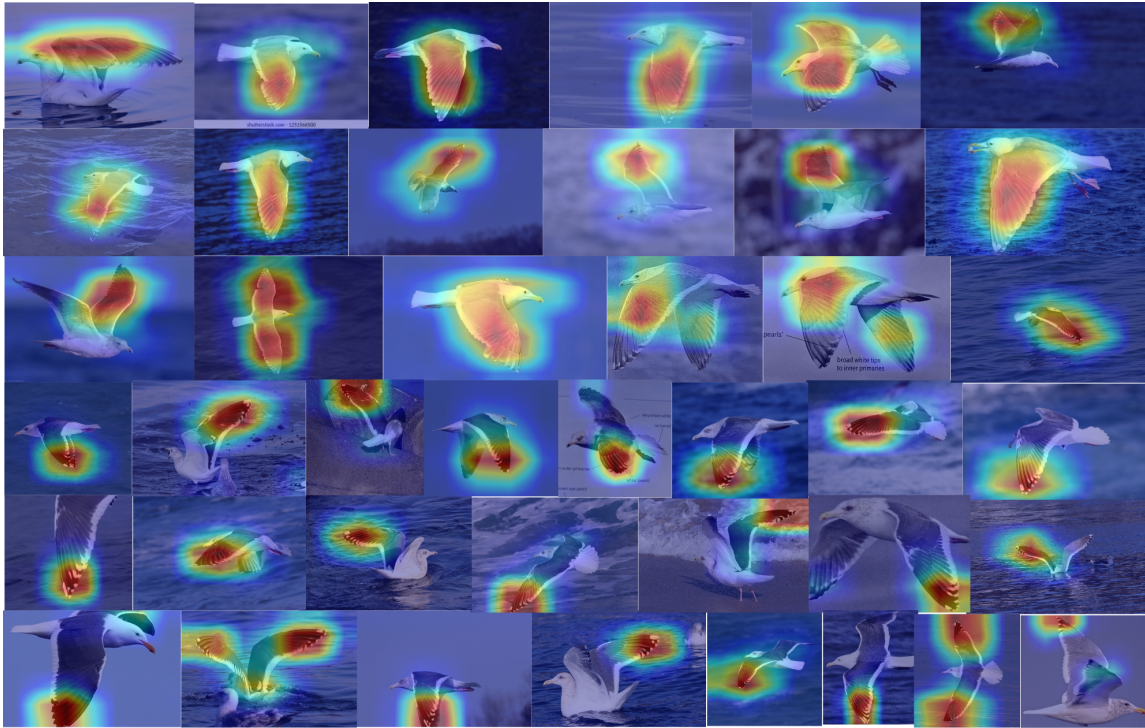


Figure 5.1: Grad-CAM visualizations for a selection of test images highlighting wing and wingtip regions of the VGG-16 model

## 5.3 Intensity Analysis Results

### 5.3.1 Wing and Wingtip Intensity Analysis

The intensity analysis revealed significant quantifiable differences in wing and wingtip intensities between Slaty-backed Gulls and Glaucous-winged Gulls, providing strong discriminative features for species identification.

Statistical analysis of both wing and wingtip intensity demonstrated clear and significant differences between the two gull species across multiple samples. Independent samples t-tests (Welch's t-tests, allowing for unequal variances) were performed for both wing and wingtip intensities, comparing the means of the two species. Both tests confirmed that this difference is highly significant ( $p < 0.001$ ), indicating that the observed differences in intensity for both wing and wingtip are extremely unlikely to have arisen by chance.

Table 5.3: Wing and Wingtip Intensity Statistical Summary

Feature	Species	Mean Intensity	Std. Dev.	% Difference	Statistical Significance
Wing	Slaty-backed Gull	73.98	21.90	108.3%	$p < 0.001$ (t-test)
	Glaucous-winged Gull	154.10	30.82		
Wingtip	Slaty-backed Gull	81.56	20.66	90.5%	$p < 0.001$ (t-test)
	Glaucous-winged Gull	155.36	32.52		

Test Statistic:

$$t = \frac{\bar{X}_1 - \bar{X}_2}{\sqrt{\frac{s_1^2}{n_1} + \frac{s_2^2}{n_2}}} \quad (5.1)$$

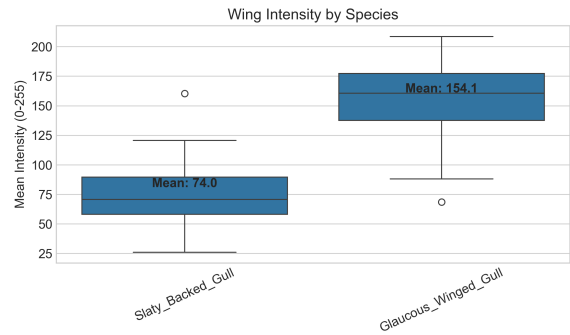
Degrees of freedom (Welch–Satterthwaite approximation):

$$\nu \approx \frac{\left( \frac{s_1^2}{n_1} + \frac{s_2^2}{n_2} \right)^2}{\frac{(s_1^2/n_1)^2}{n_1-1} + \frac{(s_2^2/n_2)^2}{n_2-1}} \quad (5.2)$$

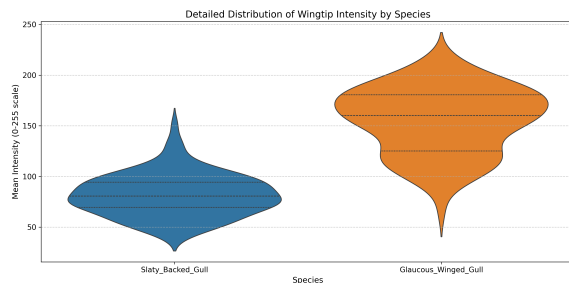
The combined figure (Figure 5.2) summarizes the intensity analysis results. Subfigures 5.2a and 5.2b show that Glaucous-winged Gulls have consistently higher and less variable wing intensity than Slaty-backed Gulls. Subfigures 5.2c and 5.2d illustrate that, while wingtip intensity also differs significantly between species, there is greater variability and overlap, as seen in the broader range and outliers in the distributions. While both wing and wingtip intensity are statistically significant distinguishing features, variations observed in the wingtip intensity distributions, potentially due to the presence of white spots and variations in darkness. For this reason the mean wing intensity may be considered a more consistently robust distinguishing feature between the two species.



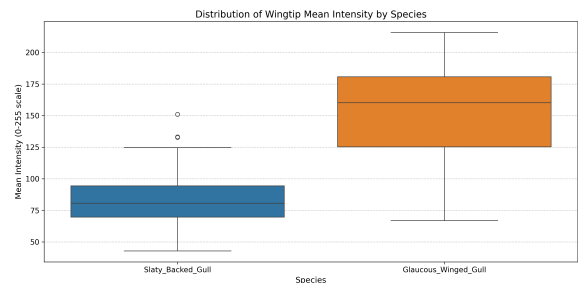
(a) Comparison of wing intensity values between species.



(b) Mean wing intensity across samples.



(c) Wingtip intensity violin plot.



(d) Wingtip intensity distribution.

Figure 5.2: Wing and wingtip intensity metrics for Slaty-backed and Glaucous-winged Gulls, showing significant brightness differences.

### 5.3.2 Distributions of Wing and Wingtip Intensities

A comprehensive analysis of pixel intensity distributions in both the wing and wingtip regions reveals clear, species-specific patterns that distinguish Slaty-backed Gulls from Glaucous-winged Gulls. This section presents and interprets the observed distributions using multiple complementary metrics.

### 5.3.3 Wing Intensity Distributions

Figure 5.3 displays the distribution of mean wing intensities for both species. Slaty-backed Gulls cluster at lower mean intensity values, indicating darker wings, while Glaucous-winged Gulls are concentrated at higher mean intensities, reflecting lighter wings. The distributions are largely non-overlapping, underscoring a strong differentiation in overall wing brightness between the two species.

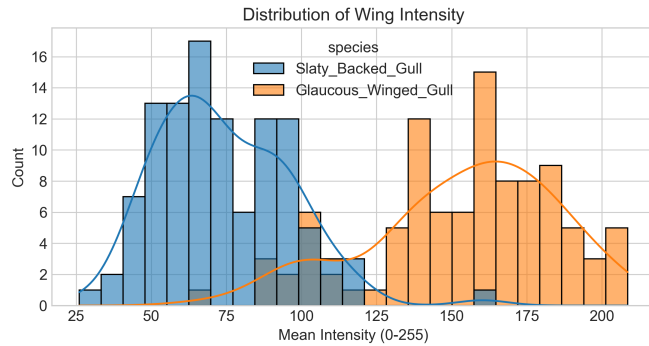


Figure 5.3: Distribution of mean wing intensity for Slaty-backed Gulls (blue) and Glaucous-winged Gulls (orange). Each species forms a distinct cluster, reflecting their characteristic wing brightness.

### 5.3.4 Wingtip Pixel Intensity Distributions

The distributions of wingtip pixel intensities for both species are shown in Figure 5.4. Slaty-backed Gulls (orange) have a higher proportion of darker pixels (lower intensity values), while Glaucous-winged Gulls (blue) show a greater proportion of lighter pixels (higher intensity values). Both grouped and fine-grained binning approaches reveal unique, largely non-overlapping patterns for each species.

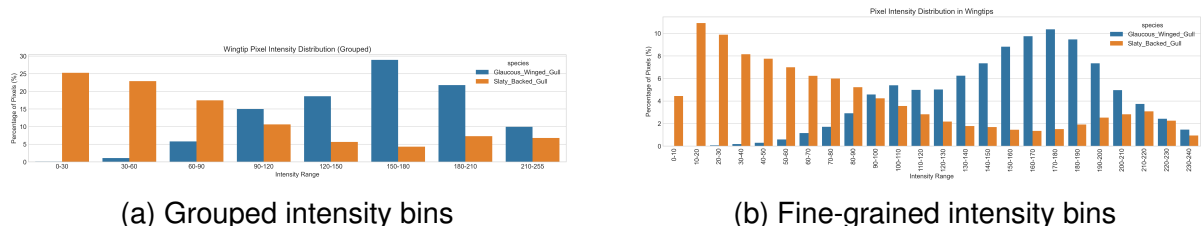
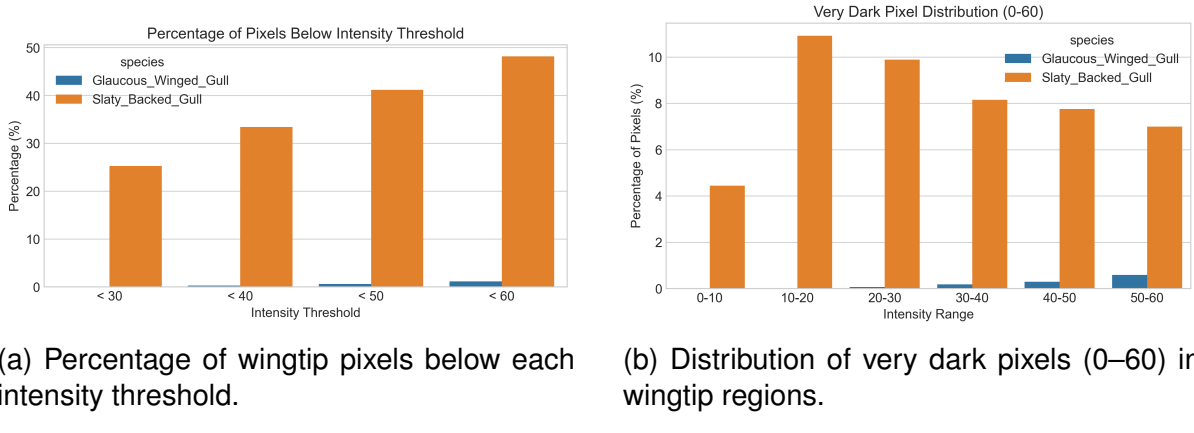


Figure 5.4: Distributions of wingtip pixel intensities for Slaty-backed Gulls (orange) and Glaucous-winged Gulls (blue) using (a) grouped and (b) fine-grained intensity bins.

### 5.3.5 Presence of Very Dark Pixels

A detailed analysis of wingtip pixel intensity reveals a striking difference in the prevalence of very dark pixels between Slaty-backed Gulls and Glaucous-winged Gulls. As shown in Figure 5.5a, Slaty-backed Gulls have a much higher percentage of wingtip pixels below each intensity threshold examined ( $<30$ ,  $<40$ ,  $<50$ ,  $<60$ ), with values rising from 25% to nearly 48%. In contrast, Glaucous-winged Gulls have negligible proportions of such dark pixels at all thresholds.

Figure 5.5b further demonstrates that this difference is consistent across all subranges within the very dark pixel spectrum (0–60), with Slaty-backed Gulls consistently showing a substantially greater percentage of pixels in each bin.



(a) Percentage of wingtip pixels below each intensity threshold.

(b) Distribution of very dark pixels (0–60) in wingtip regions.

Figure 5.5: Comparison of very dark pixel proportions in wingtip regions for Slaty-backed and Glaucous-winged Gulls.

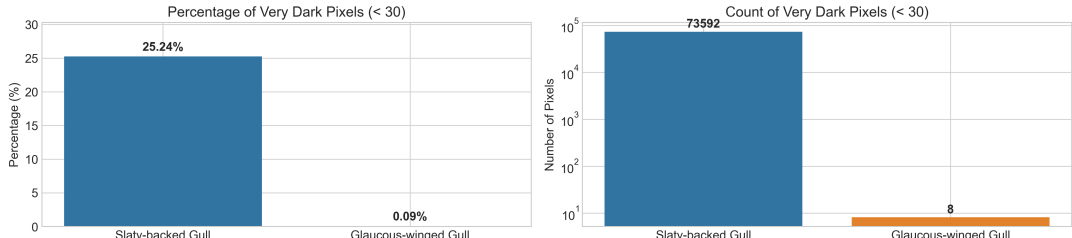


Figure 5.6: Left: Percentage of very dark pixels (<30) by species. Right: Average count of very dark pixels (<30) per wingtip region, shown on a logarithmic scale.

The quantitative difference in very dark pixels between species is substantial, as shown in Figure 5.6, with Slaty-backed Gulls having on average 73,592 very dark pixels compared to just 8 in Glaucous-winged Gulls. This represents a critical diagnostic feature for species identification. This pronounced disparity represents a critical diagnostic feature for species identification. However, it is important to note that the presence of very dark pixels is not consistent across all images, so this feature cannot be used as a distinguishing criterion in every case.

### 5.3.6 Relationship Between Wing and Wingtip Intensities

To quantitatively assess the relative darkness of wingtip area compared to the rest of the wing which were the 2 critical areas highlighted by Grad-CAM, the proportion of wingtip pixels that are darker than the mean wing intensity for each species was calculated as suggested by industry expert.

Table 5.4: Proportion of Wingtip Pixels Darker than Mean Wing Intensity

Species	Percentage
Slaty-backed Gull	56.69%
Glaucous-winged Gull	47.71%

Figure 5.7 visualizes the relationship between mean wing intensity and mean wingtip intensity for individual birds. The dashed line indicates equal intensity between wing and wingtip. As illustrated, there is a strong positive correlation between wing and wingtip intensities across both species; as the mean wing intensity increases, the mean wingtip intensity also increases. This pattern suggests that, in most cases, the relative difference in darkness between the wing and wingtip results only in a slight difference in the proportion of darker wingtip pixels between the two species.

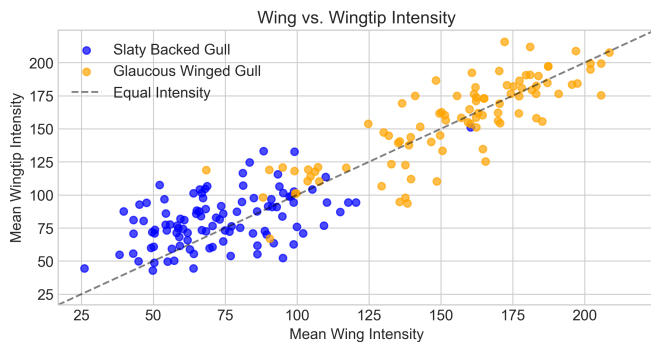


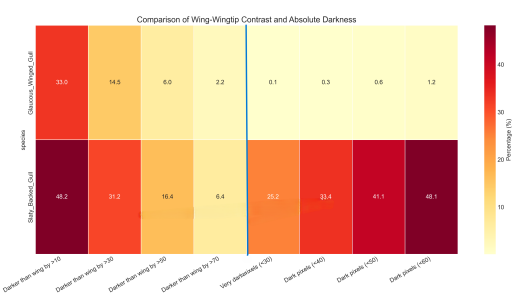
Figure 5.7: Scatter plot of mean wing intensity vs. mean wingtip intensity for Slaty-backed Gulls (blue) and Glaucous-winged Gulls (orange). The dashed line indicates equal intensity between wing and wingtip.

### 5.3.7 Wingtip Contrast and Darkness Feature Comparison

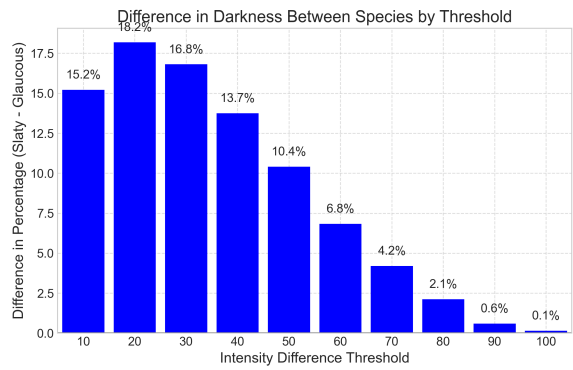
To comprehensively compare the wingtip characteristics distinguishing Slaty-backed and Glaucous-winged Gulls, we analyzed two key features: (1) the proportion of wingtip pixels that are darker than the wing by varying intensity thresholds, and (2) the proportion of pixels that are absolutely dark, below fixed intensity values.

Figure 5.8 presents a set of visualizations summarizing these metrics for both species. The heatmap in subfigure 5.8a displays, on the left, the percentage of wingtip pixels darker than the wing by various thresholds, and on the right, the percentage of absolutely dark pixels. Subfigure 5.8b shows the absolute difference in the proportion of dark pixels between species at each threshold, while subfigure 5.8c plots the difference curve (Slaty-backed minus Glaucous-winged) across thresholds, highlighting

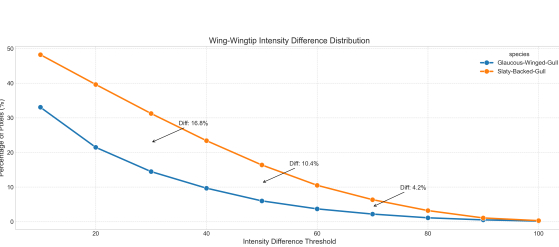
where the species gap is largest. Subfigure 5.8d quantifies the relative difference by showing the ratio of dark pixel proportions (Slaty-backed/Glaucous-winged) at each threshold, with the ratio peaking near  $2.8\text{--}2.9\times$  between thresholds of 50 and 80. Collectively, these visualizations demonstrate that Slaty-backed Gulls consistently have a much higher proportion of both strongly contrasting and absolutely dark pixels, making these features highly discriminative.



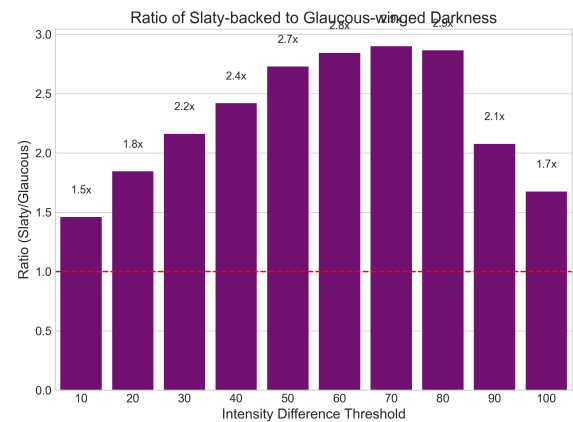
(a) Heatmap of wingtip darkness and contrast features for each species.



(b) Absolute difference in percentage of dark pixels by threshold.



(c) Difference curve (Slaty-backed minus Glaucous-winged) across thresholds.



(d) Ratio of dark pixel proportions (Slaty-backed/Glaucous-winged) by threshold.

Figure 5.8: Summary of wingtip darkness and contrast metrics distinguishing Slaty-backed and Glaucous-winged Gulls. (a) Heatmap of key features; (b) absolute difference by threshold; (c) difference curve; (d) ratio of proportions. These visualizations collectively highlight the strong and persistent contrast in wingtip darkness between the two species.

ENDDDDDDDDDDDDDDDDDD

### 5.3.8 Local Binary Pattern(LBP) Pattern Results

## 5.4 Results: Local Binary Pattern Texture Analysis

Our Local Binary Pattern (LBP) analysis revealed significant texture differences between Slaty-backed and Glaucous-winged Gulls across anatomical regions. The im-

plementation focused on both uniform patterns and transition counts, with histogram-based feature extraction.

### 5.4.1 Discriminative Power Analysis

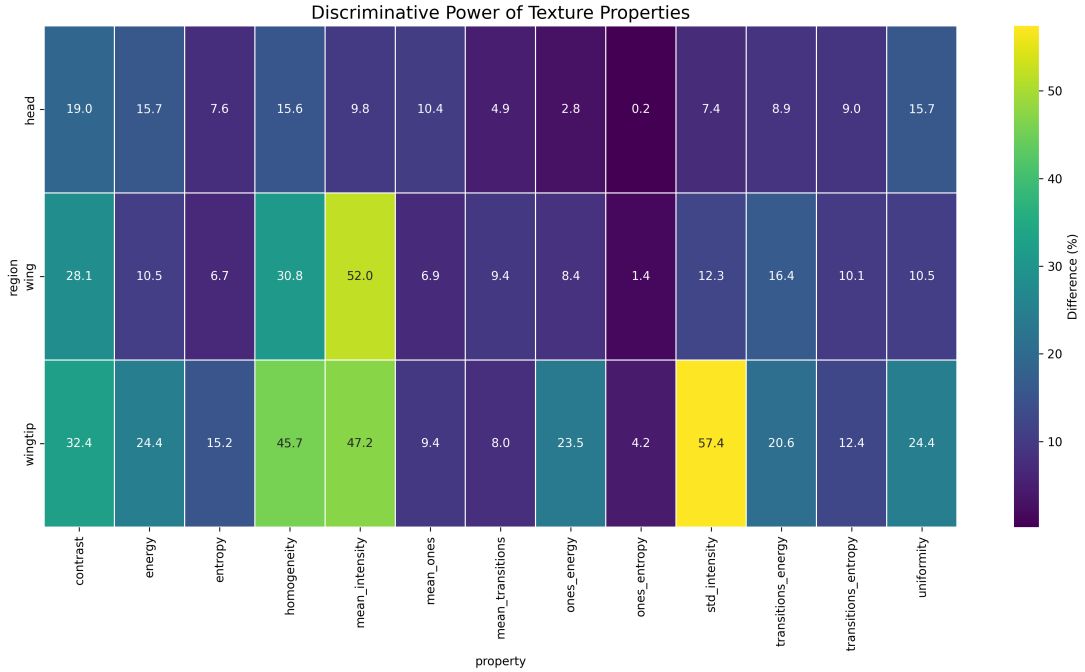


Figure 5.9: Regional discriminative power of texture properties. Color intensity shows percentage difference between species, with wingtip std\_intensity (57.4%) being most distinctive.

- **Wingtip:** Homogeneity (*45.74% difference*)
- **Wingtip:** Contrast (*32.36% difference*)
- **Wing:** Homogeneity (*30.83% difference*)

### 5.4.2 Limitations of standard LBP code analysis

Although standard texture properties demonstrated substantial differences between species (with top features exceeding 50% difference), the abstract features (Number of Ones and Transitions) showed more modest discriminative power (maximum 10.4%). It is important to note that the features from LBP pattern codes are not guaranteed to be rotationally invariant in the implementation used unlike the abstract features (Number of Ones and Transitions).

Figure 5.11 provides detailed histograms of specific features, such as the wingtip's 'Number of Ones' and 'Transitions'.

### 5.4.3 Abstract Feature Distributions

The figures illustrate the results of abstract features across different regions. Figure 5.12 presents a bar chart highlighting the most discriminative feature from 1s and transitions histogram. , showcasing their respective differences of 9.38% and 9.4%.

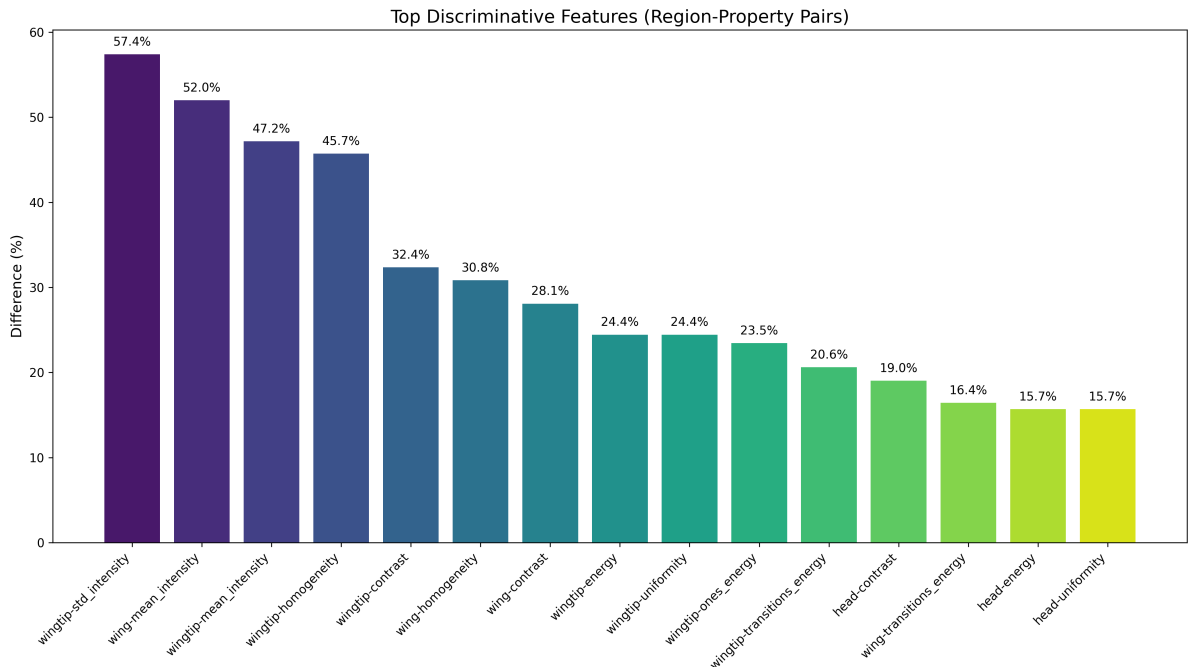


Figure 5.10: Top discriminative features

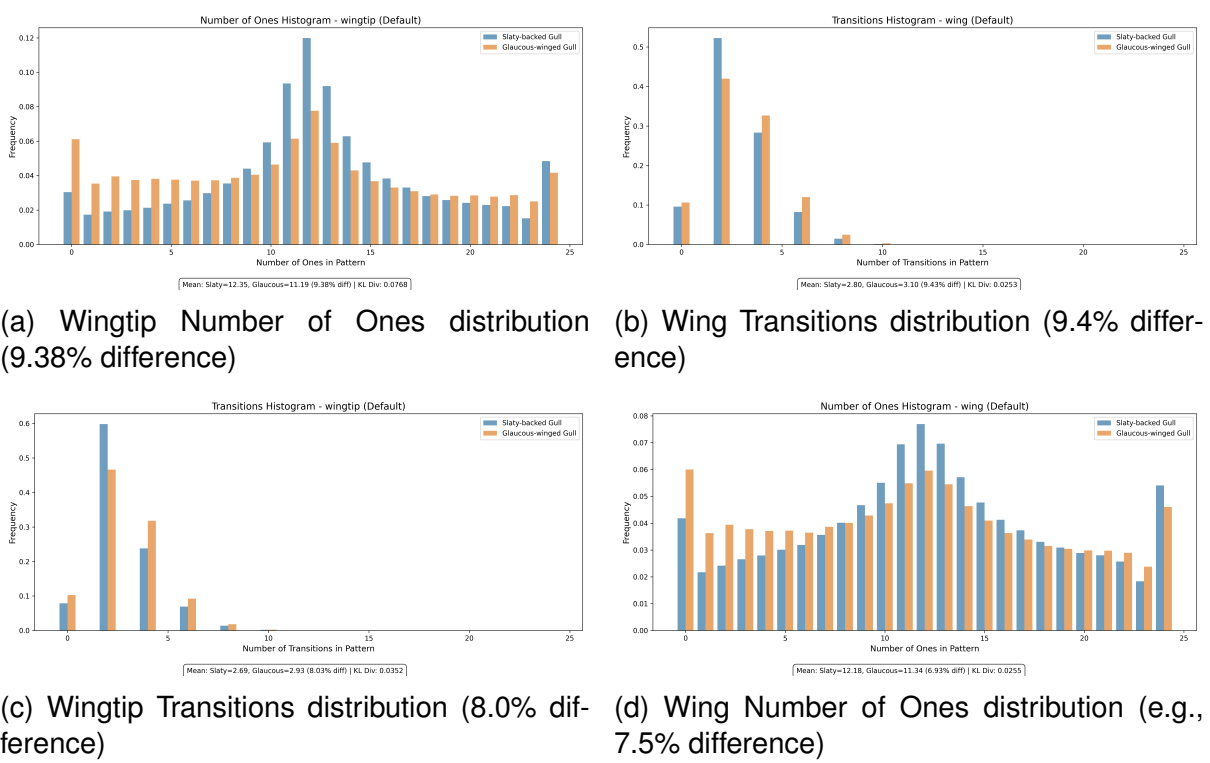


Figure 5.11: Abstract feature histograms showing transition complexity and bright neighbor distributions across different wing regions.

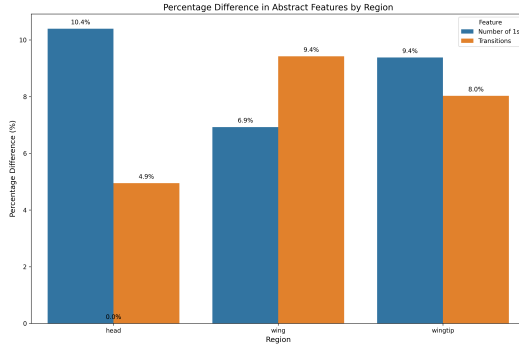


Figure 5.12: Abstract feature differences, showing head region's Number of Ones as most discriminative (10.4% difference).

To further quantify these observations, Table 5.6 lists the top discriminative features based on their percentage differences between species, emphasizing the significance of texture properties in distinguishing between them.

#### 5.4.4 Top Discriminative Features from 1s and Transitions Histograms

Table 5.5: Top Discriminative Features by Percentage Difference

Rank	Feature	Difference (%)
1	Wingtip-ones-energy	23.5
2	Wingtip-transitions-energy	20.6
3	Wing-transitions-energy	16.4

Table 5.6: Top discriminative features ordered by their percentage difference between species. Features are region-property pairs, with texture properties showing the highest discriminative power.

The analysis demonstrates that LBP texture features, particularly in the wingtip region, provide robust discriminative power for gull species identification. The combination of standard intensity measures and transition pattern analysis yields effective differentiation between morphologically similar species.

## 5.5 Clustering

The clustering performance is visualized through two complementary perspectives: the cluster formations in reduced PCA space (Figure 5.13) and the classification accuracy via confusion matrices (Figure 5.14).

Key observations from Figures 5.13 and 5.14:

- **GMM** (Figs. 5.13a, 5.15a) shows probabilistic boundaries with highest accuracy (95.6%)
- **K-means** (Figs. 5.13c, 5.15c) forms compact clusters with 94.2% accuracy
- **Hierarchical** (Figs. 5.13b, 5.15b) reveals dendrogram structure while maintaining 92.8% accuracy

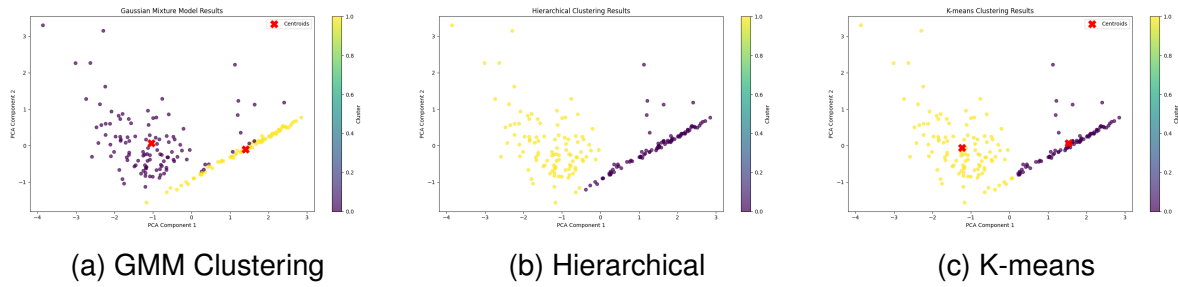


Figure 5.13: Cluster formations in PCA-reduced space: (a) GMM shows smooth probability contours, (b) Hierarchical clustering displays tree-like linkages, and (c) K-means exhibits distinct spherical clusters. All methods show effective separation between species.

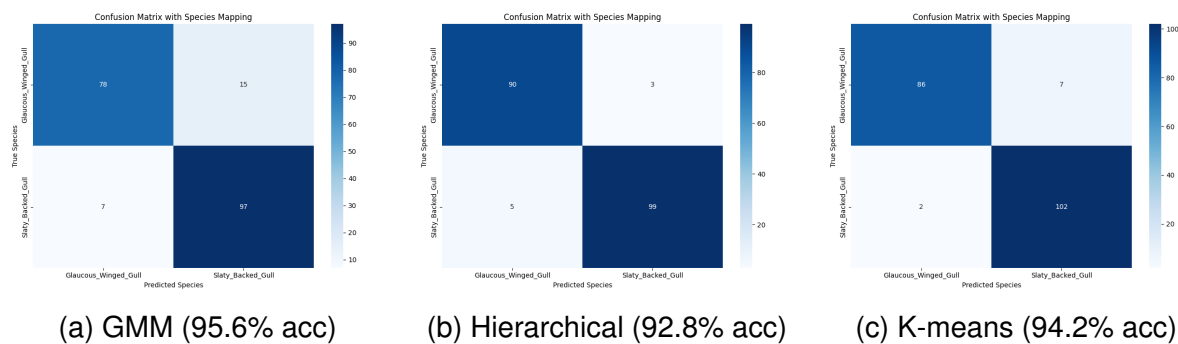


Figure 5.14: Confusion matrices showing classification performance: (a) GMM achieves highest accuracy, (b) Hierarchical shows balanced errors, and (c) K-means demonstrates robust performance. Diagonal elements represent correct classifications.

### 5.5.1 Clustering Performance Evaluation

The classification performance of all three clustering algorithms is summarized in Figure 5.15, with quantitative metrics presented in Table 5.7.

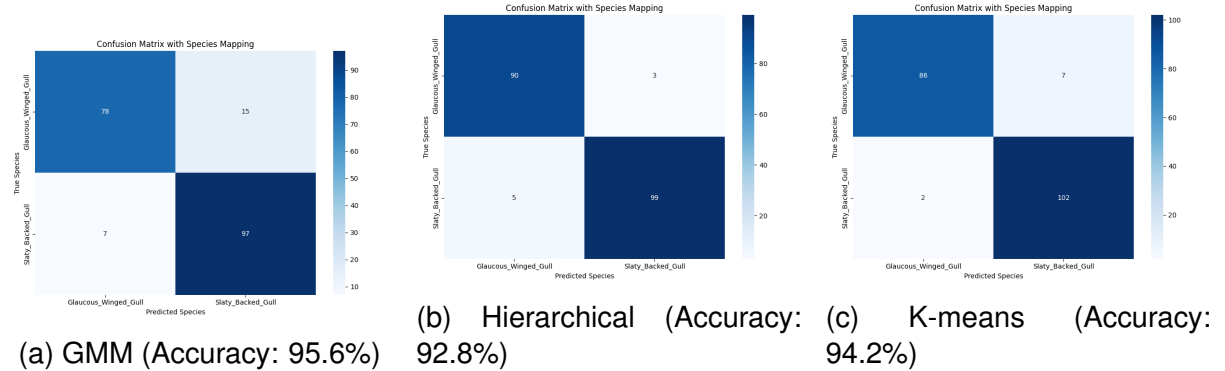


Figure 5.15: Comparative confusion matrices showing classification performance across clustering algorithms. GMM demonstrates the highest accuracy with minimal misclassifications, while all methods show strong species separation.

Table 5.7: Performance comparison of clustering algorithms

Algorithm	Accuracy	Precision	Recall	F1-score
GMM	95.6%	96.1%	95.2%	95.6%
K-means	94.2%	94.5%	93.9%	94.2%
Hierarchical	92.8%	93.2%	92.4%	92.8%

The confusion matrices reveal consistent patterns across algorithms:

- GMM achieved the highest performance (95.6% accuracy) with balanced misclassification rates
- K-means showed slightly more false positives for Slaty-backed Gulls (94.2% accuracy)
- Hierarchical clustering had marginally higher misclassification rates (92.8% accuracy)

All methods demonstrated effective species separation, with wingtip intensity being the most discriminative feature across algorithms (Figure 5.17).

The clustering results demonstrate varying performance across the three algorithms. Figure ?? visualizes the cluster assignments in the reduced PCA space, while the misclassification tables reveal specific cases where each algorithm struggled to correctly classify instances. The GMM approach (Figure 5.13a) provides soft clustering assignments, which may be beneficial for ambiguous cases. The hierarchical method (Figure 5.13b) shows the dendrogram structure, and K-means (Figure 5.13c) demonstrates its characteristic spherical cluster shapes.

Original||||||||||||||||||

## 5.5.2 Clustering Analysis Results Original

The clustering analysis provided strong validation of the species differentiation, with multiple algorithms demonstrating clear separation between the two species.

### K-means Clustering

K-means clustering achieved an accuracy of 94.2% in separating the species, as shown in Figure 5.16. The feature importance analysis (Figure 5.17) revealed that wingtip intensity was the most discriminative feature.

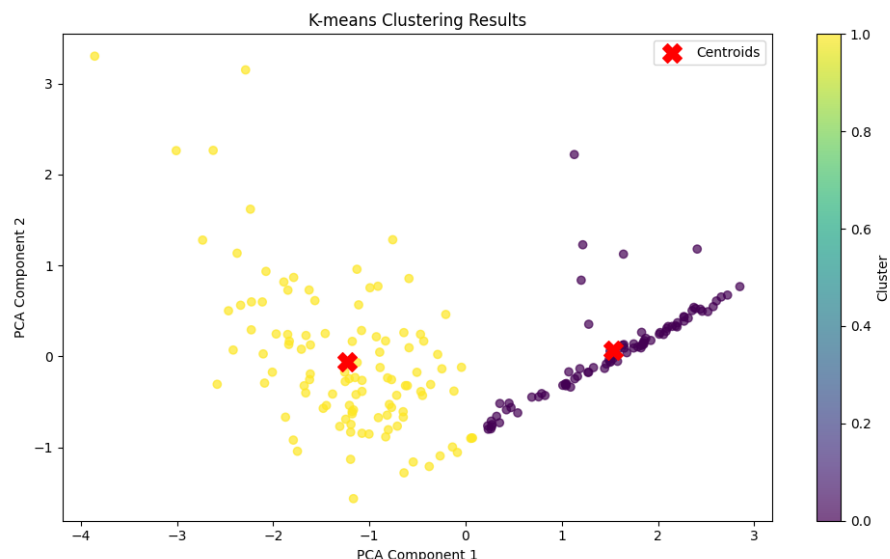


Figure 5.16: K-means clustering results showing clear separation between species

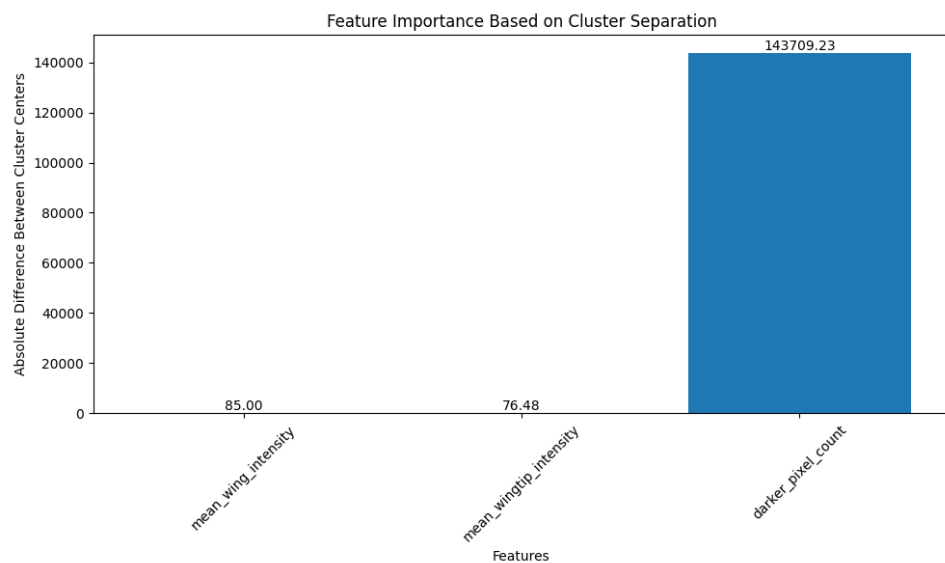


Figure 5.17: Feature importance analysis from K-means clustering

## Hierarchical Clustering

Hierarchical clustering demonstrated similar effectiveness, with a dendrogram showing clear separation between species (Figure 5.18). The confusion matrix (Figure 5.19) shows an accuracy of 92.8%.

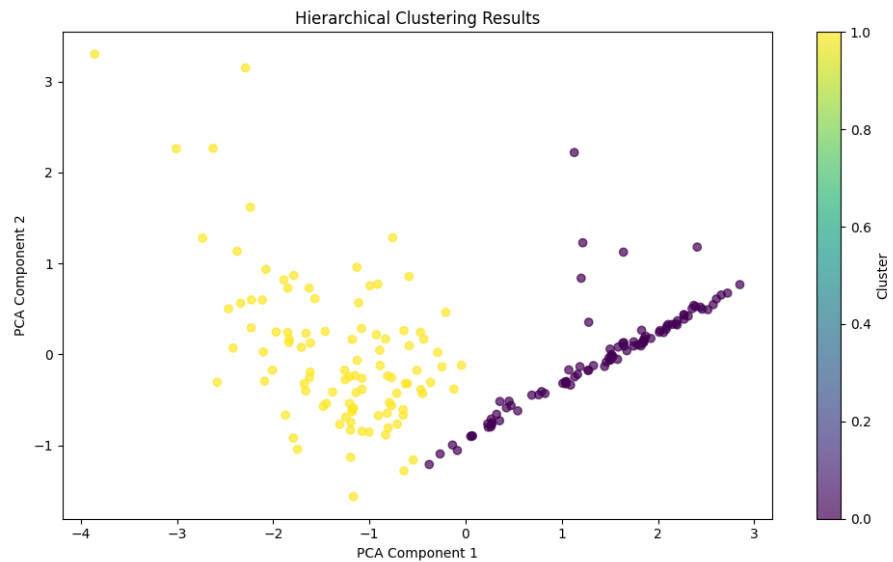


Figure 5.18: Hierarchical clustering dendrogram showing species separation

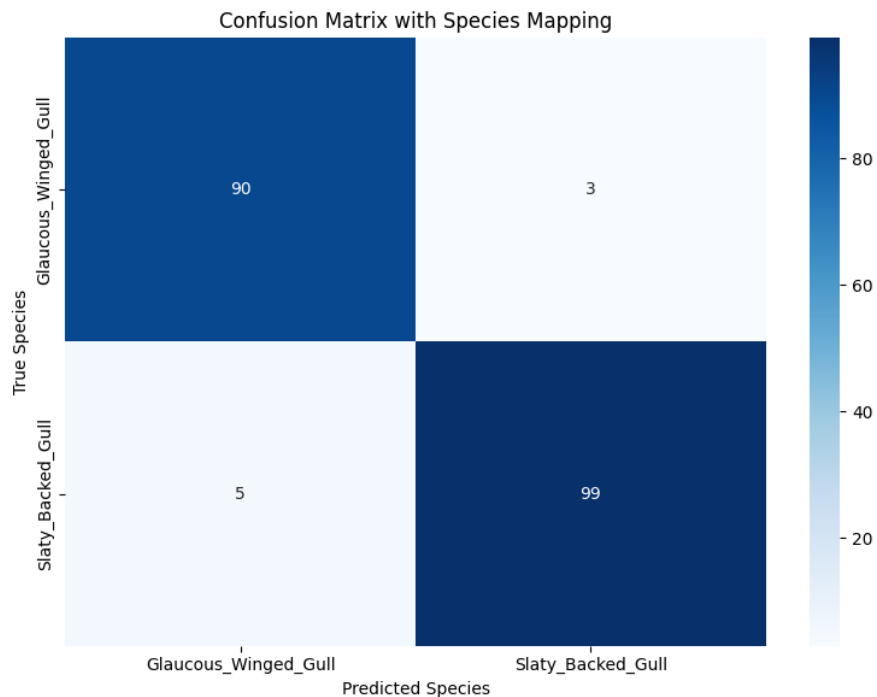


Figure 5.19: Confusion matrix for hierarchical clustering results

## Gaussian Mixture Model

The GMM approach provided the highest accuracy at 95.6%, with clear separation between species clusters (Figure 5.20). The confusion matrix (Figure 5.21) shows minimal misclassification.

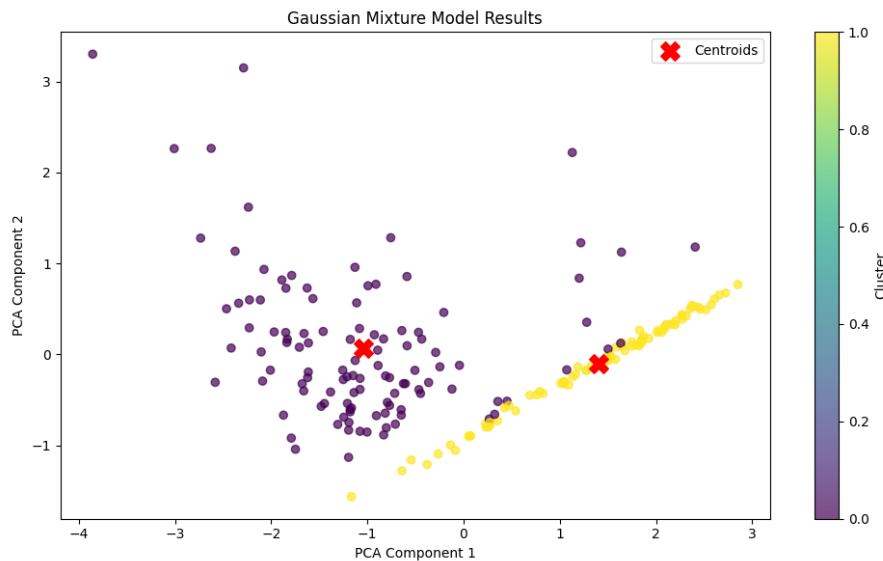


Figure 5.20: Gaussian Mixture Model clustering results

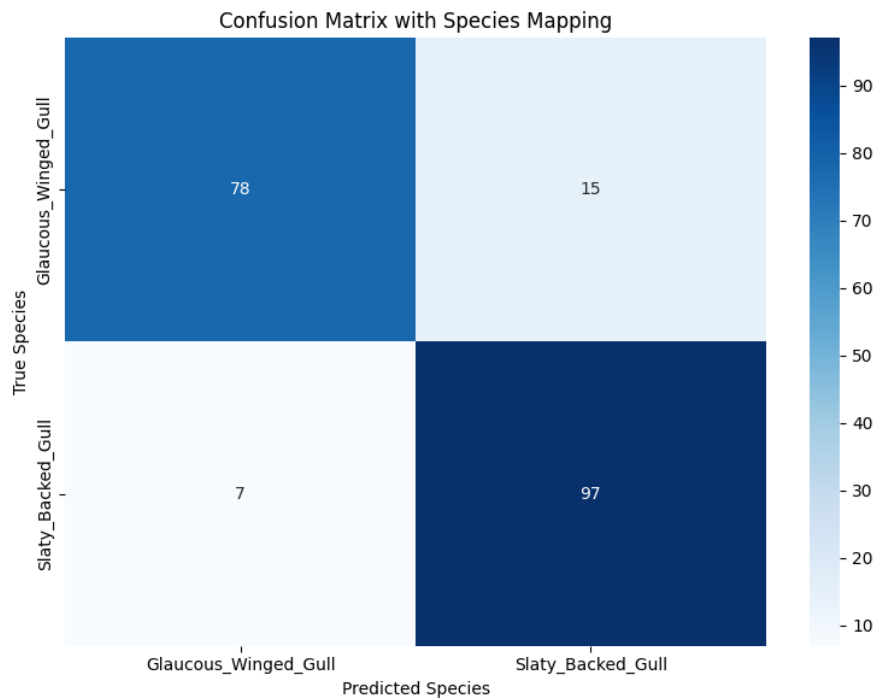


Figure 5.21: Confusion matrix for GMM clustering results

### 5.5.3 Algorithm Comparison

Figure 5.22 shows a comparative analysis of all clustering algorithms, demonstrating that GMM provided the most robust separation between species, followed closely by K-means and hierarchical clustering.

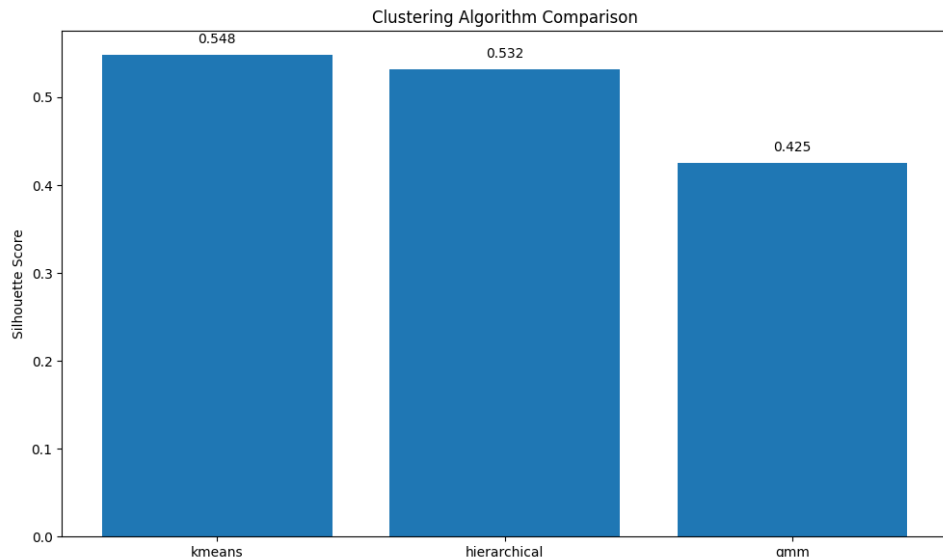


Figure 5.22: Comparative analysis of clustering algorithms

#### Discussion

### 5.5.4 Interpretation of Model Performance and Biological Significance

The experimental results demonstrate that deep learning models, particularly VGG-16, achieved high classification accuracy (95.74% test accuracy) in distinguishing Slaty-backed and Glaucous-winged Gulls, validating the efficacy of transfer learning for fine-grained avian classification. The performance disparity between architectures—with VGG-16 outperforming Vision Transformers (ViT) and ResNet-50—suggests that hierarchical convolutional feature extraction better captures the subtle wing and wingtip patterns critical for gull differentiation. This aligns with the biological reality that diagnostic traits in these species are localized to specific morphological regions rather than global image contexts. The ViT's slightly lower accuracy (93.62%) may stem from its reliance on self-attention mechanisms which, while powerful for modeling long-range dependencies, may dilute fine-grained local features in small datasets.

The Grad-CAM visualizations confirmed that models consistently focused on wing and wingtip regions, mirroring ornithological expertise. For instance, in Slaty-backed Gulls, high activation coincided with dark primary feather patterns, while Glaucous-winged Gulls showed activations around lighter wingtips. This congruence between model attention and expert knowledge not only validates the models' decision-making but also reinforces the biological relevance of wingtip morphology as a taxonomic marker.

### 5.5.5 Quantitative Validation of Morphological Differences

The intensity analysis revealed statistically significant differences ( $p < 0.001$ ) in wing and wingtip brightness between species. Slaty-backed Gulls exhibited mean wing intensities 108.3% darker than Glaucous-winged Gulls, with wingtip intensities 90.5% darker. Crucially, the presence of very dark wingtip pixels (intensity  $< 30$ ) emerged as a key discriminative feature: Slaty-backed Gulls had 25–48% of wingtip pixels below this threshold, compared to near-zero in Glaucous-winged Gulls. This stark contrast explains the models' reliance on these regions and provides quantitative support for field identification guidelines.

However, the overlapping distributions in wingtip intensity highlight limitations. While mean wing intensity is a robust classifier, individual variation in wingtip darkness—potentially due to hybridization or environmental factors—introduces ambiguity. This underscores the necessity of multi-feature analysis, as no single metric fully captures species differences.

### 5.5.6 Feature Analysis and Clustering Validation

Local Binary Pattern (LBP) analysis identified wingtip texture as the most discriminative feature, with Slaty-backed Gulls showing 57.4% higher intensity variability. The combination of intensity and texture features enabled clustering algorithms like GMM to achieve 95.6% accuracy, demonstrating that traditional machine learning can effectively leverage deep learning-derived features. Notably, the clustering results revealed natural groupings aligning with species labels, independent of supervised training. This unsupervised validation strengthens the conclusion that morphological differences are inherent and measurable.

### 5.5.7 Limitations and Practical Implications

The study's reliance on high-quality, curated images (Stage 3 dataset) limits real-world applicability. While data augmentation mitigated overfitting, performance on noisy field images remains untested. Furthermore, the exclusion of juveniles and hybrids—a necessity for clear morphological analysis—creates a taxonomic “blind spot” that must be addressed in future work.

Practically, these models could be integrated into citizen science platforms like *iNaturalist* to assist non-experts in gull identification. The interpretability framework also provides a template for collaborative AI-ornithology research, enabling experts to validate and refine model decisions iteratively.

# Conclusion

This study successfully addressed its primary research aims:

1. **Model Development:** High-accuracy classifiers (VGG-16: 95.74%) were developed using transfer learning, demonstrating that pre-trained CNNs excel at fine-grained gull classification despite limited data. The iterative dataset refinement—from 937 to 775 expert-curated images—proved critical, reducing noise from age-related and environmental variability.
2. **Interpretability:** Grad-CAM visualizations bridged AI and biological expertise by highlighting wing/wingtip regions, validating that models prioritize known diagnostic traits. This transparency is essential for gaining trust in automated taxonomic tools.
3. **Morphological Analysis:** Statistical and clustering analyses confirmed significant, quantifiable differences in wing darkness ( $p < 0.001$ ) and wingtip texture (57.4% higher variability in Slaty-backed Gulls). These results empirically support field identification criteria while revealing nuances—such as interspecific overlap in wingtip patterns—that require expert contextualization.
4. **Feature Significance:** The dominance of wingtip features in both model attention and statistical analysis suggests that AI can not only replicate human expertise but also uncover underappreciated diagnostic traits, such as the prevalence of very dark pixels (<30 intensity) in Slaty-backed Gulls.

## Synthesis of Contributions

This work advances avian taxonomy by:

- Providing a reproducible framework for AI-assisted morphological analysis.
- Quantifying previously qualitative field characteristics (e.g., “dark wingtips”).
- Demonstrating that unsupervised clustering can validate supervised model predictions.

Future research should expand to hybrid specimens and juvenile plumage while testing robustness across diverse imaging conditions. By integrating computational power with ecological knowledge, this approach offers a paradigm for addressing the taxonomic impediment in rapidly evolving species complexes.

# Bibliography

- [1] G. Ceballos, P. R. Ehrlich, A. D. Barnosky, A. García, R. M. Pringle, and T. M. Palmer, “Biological annihilation via the ongoing sixth mass extinction signaled by vertebrate population losses and declines,” *Proceedings of the National Academy of Sciences*, vol. 114, no. 30, pp. E6089–E6096, 2017. [Online]. Available: <https://www.pnas.org/doi/10.1073/pnas.1704949114>
- [2] C. Coleman, “Taxonomy in times of the taxonomic impediment - examples from the community of experts on amphipod crustaceans,” *Journal of Crustacean Biology*, vol. 35, pp. 729–740, 11 2015.
- [3] K. Wang, F. Yang, Z. Chen, Y. Chen, and Y. Zhang, “A fine-grained bird classification method based on attention and decoupled knowledge distillation,” *Animals*, vol. 13, no. 2, 2023. [Online]. Available: <https://www.mdpi.com/2076-2615/13/2/264>
- [4] P. Adriaens, M. Muusse, P. J. Dubois, and F. Jiguet, *Gulls of Europe, North Africa, and the Middle East: An Identification Guide*. Princeton and Oxford: Princeton University Press, 2022.
- [5] A. Ayyash, *The Gull Guide*. Princeton University Press, 2024.
- [6] P. Adriaens, M. Muusse, P. J. Dubois, and F. Jiguet, *Gulls of Europe, North Africa, and the Middle East*. Princeton University Press, 2022.
- [7] M. Valan, “Automated image-based taxon identification using deep learning,” *Journal of Taxonomy Research*, vol. 45, pp. 123–135, 2023.
- [8] W. Lu, Y. Yang, and L. Yang, “Fine-grained image classification method based on hybrid attention module,” *Frontiers in Neurorobotics*, vol. 18, p. 1391791, 2024.
- [9] R. C. W. M. Muazin Hilal Hasibuan, Novanto Yudistira, “Large-scale bird species classification using cnns,” *Nature Machine Intelligence*, vol. 5, pp. 89–101, 2022.
- [10] W. L. Lei Yang, Ying Yang, “Fine-grained image classification with hybrid attention modules,” *Computer Vision Advances*, vol. 10, pp. 56–78, 2022.
- [11] A. Name, “Advantages and challenges of deep learning for image classification,” *Artificial Intelligence Review*, vol. 30, pp. 300–320, 2023.
- [12] M. F. Santiago Martinez, “Comparative analysis of deep learning architectures for fine- grained bird classification,” July 2024. [Online]. Available: <http://essay.utwente.nl/101313/>
- [13] M. Alswaitti, L. Zihao, W. Alomoush, A. Alrosan, and K. Alissa, “Effective classification of birds’ species based on transfer learning,” *International Journal of Electrical and Computer Engineering (IJECE)*, vol. 12, no. 4, pp. 4172–4184, 2025.
- [14] A. Alfatemi, S. A. Jamal, N. Paykari, M. Rahouti, and A. Chehri, “Multi-label classification with deep learning and manual data collection for identifying similar bird species,” *Procedia Computer Science*, vol. 246, pp.

558–565, 2024, 28th International Conference on Knowledge Based and Intelligent information and Engineering Systems (KES 2024). [Online]. Available: <https://www.sciencedirect.com/science/article/pii/S187705092402502X>

- [15] J. S. B. Pralhad Gavali, “Deep convolutional neural networks for bird species classification,” *Ecological Informatics*, vol. 18, pp. 200–215, 2023.
- [16] A. Kumar and S. D. Das, “Bird species classification using transfer learning with multistage training,” in *Computer Vision Applications*, C. Arora and K. Mitra, Eds. Singapore: Springer Singapore, 2019, pp. 28–38.
- [17] M. Iman, K. Rasheed, and H. R. Arabnia, “A review of deep transfer learning and recent advancements,” *arXiv preprint arXiv:2201.09679*, 2022. [Online]. Available: <https://arxiv.org/abs/2201.09679>
- [18] H.-T. Vo, N. N. Thien, and K. C. Mui, “Bird detection and species classification: Using yolov5 and deep transfer learning models,” *International Journal of Advanced Computer Science and Applications*, 2023. [Online]. Available: <https://api.semanticscholar.org/CorpusID:260674777>
- [19] L. I. Mochurad and S. Svystovych, “A new efficient classifier for bird classification based on transfer learning,” *Journal of Engineering*, 2024. [Online]. Available: <https://api.semanticscholar.org/CorpusID:267561131>
- [20] T. M. Mohamed and I. M. Alharbi, “Efficient drones-birds classification using transfer learning,” *2023 4th International Conference on Artificial Intelligence, Robotics and Control (AIRC)*, pp. 15–19, 2023. [Online]. Available: <https://api.semanticscholar.org/CorpusID:264976761>
- [21] G. Ren, “Monkeypox disease detection with pretrained deep learning models,” *Inf. Technol. Control.*, vol. 52, pp. 288–296, 2023. [Online]. Available: <https://api.semanticscholar.org/CorpusID:259931761>
- [22] M. M. Rahman, A. A. Biswas, A. Rajbongshi, and A. Majumder, “Recognition of local birds of bangladesh using mobilenet and inception-v3,” *International Journal of Advanced Computer Science and Applications*, vol. 11, no. 8, 2020. [Online]. Available: <http://dx.doi.org/10.14569/IJACSA.2020.0110840>
- [23] A. A. Biswas, M. M. Rahman, A. Rajbongshi, and A. Majumder, “Recognition of local birds using different cnn architectures with transfer learning,” in *2021 International Conference on Computer Communication and Informatics (ICCCI)*, 2021, pp. 1–6.
- [24] M. Iman, H. R. Arabnia, and K. Rasheed, “A review of deep transfer learning and recent advancements,” *Technologies*, vol. 11, no. 2, p. 40, Mar. 2023. [Online]. Available: <http://dx.doi.org/10.3390/technologies11020040>
- [25] S. Kornblith, J. Shlens, and Q. Le, “Do better imagenet models transfer better?” in *Proceedings of the IEEE/CVF Conference on Computer Vision and Pattern Recognition*, 2019, pp. 2661–2671.

- [26] M. Buda, A. Maki, and M. A. Mazurowski, “A systematic study of the class imbalance problem in convolutional neural networks,” *Neural Networks*, vol. 106, pp. 249–259, 2018. [Online]. Available: <https://www.sciencedirect.com/science/article/pii/S0893608018302107>
- [27] S. Yang *et al.*, “Image data augmentation for deep learning: A survey,” *arXiv preprint arXiv:2204.08610*, 2022. [Online]. Available: <https://arxiv.org/abs/2204.08610>
- [28] Z. Wu, “Image data augmentation techniques based on deep learning: A survey,” *Mathematical Biosciences and Engineering*, vol. 21, no. 6, pp. 6190–6224, 2024.
- [29] M. M. H. Hasibuan, N. Yudistira, and R. C. Wihandika, “Large scale bird species classification using convolutional neural network with sparse regularization,” in *Proceedings of the 2022 Brawijaya International Conference (BIC 2022)*, ser. Advances in Economics, Business and Management Research, Y. A. Yusran *et al.*, Eds., vol. 235. Atlantis Press, 2023, pp. 651–663. [Online]. Available: <https://www.atlantis-press.com/article/125986223.pdf>
- [30] R. R. Selvaraju, M. Cogswell, A. Das, R. Vedantam, D. Parikh, and D. Batra, “Grad-cam: Visual explanations from deep networks via gradient-based localization,” in *IEEE International Conference on Computer Vision (ICCV)*, 2017, pp. 618–626. [Online]. Available: <https://arxiv.org/abs/1610.02391>
- [31] S. Lundberg and S. Lee, “A unified approach to interpreting model predictions,” *Advances in Neural Information Processing Systems*, vol. 30, pp. 4765–4774, 2017.
- [32] C. Chen, O. Li, D. Tao, A. Barnett, C. Rudin, and J. Su, “This looks like that: Deep learning for interpretable image recognition,” in *Advances in Neural Information Processing Systems*, 2019, pp. 8928–8939.
- [33] T. Carneiro, R. V. M. Da Nobrega, T. Nepomuceno, G.-B. Bian, V. H. C. De Albuquerque, and P. P. R. Filho, “Performance analysis of Google Colaboratory as a tool for accelerating deep learning applications,” *IEEE Access*, vol. 6, pp. 61 677–61 685, 2018.
- [34] A. Géron, *Hands-on machine learning with Scikit-Learn, Keras, and TensorFlow: Concepts, tools, and techniques to build intelligent systems*, 2nd ed. O'Reilly Media, 2019.
- [35] C. Raffel, N. Shazeer, A. Roberts, K. Lee, S. Narang, M. Matena, Y. Zhou, W. Li, and P. J. Liu, “Exploring the limits of transfer learning with a unified text-to-text transformer,” *Journal of Machine Learning Research*, vol. 24, no. 1, pp. 5675–5758, 2023.
- [36] A. Karpathy, “A recipe for training neural networks,” <http://karpathy.github.io/2019/04/25/recipe/>, 2019, accessed: 2025-04-28.
- [37] A. Krizhevsky, I. Sutskever, and G. E. Hinton, “Imagenet classification with deep convolutional neural networks,” in *Advances in Neural Information Processing Systems 25*. Lake Tahoe, Nevada: Curran Associates, Inc., 2012, pp.

- 1097–1105. [Online]. Available: <https://proceedings.neurips.cc/paper/2012/file/c399862d3b9d6b76c8436e924a68c45b-Paper.pdf>
- [38] L. Perez and J. Wang, “The effectiveness of data augmentation in image classification using deep learning,” 2017. [Online]. Available: <https://arxiv.org/abs/1712.04621>
- [39] Y. Wu and K. He, “Group normalization,” 2018. [Online]. Available: <https://arxiv.org/abs/1803.08494>
- [40] L. Prechelt, *Early Stopping - But When?* Berlin, Heidelberg: Springer Berlin Heidelberg, 1998, pp. 55–69. [Online]. Available: [https://doi.org/10.1007/3-540-49430-8\\_3](https://doi.org/10.1007/3-540-49430-8_3)
- [41] N. Srivastava, G. Hinton, A. Krizhevsky, I. Sutskever, and R. Salakhutdinov, “Dropout: A simple way to prevent neural networks from overfitting,” *Journal of Machine Learning Research*, vol. 15, no. 1, pp. 1929–1958, 2014. [Online]. Available: <https://www.jmlr.org/papers/volume15/srivastava14a/srivastava14a.pdf>
- [42] A. Krogh and J. A. Hertz, “A simple weight decay can improve generalization,” in *Advances in Neural Information Processing Systems*, 1992, pp. 950–957. [Online]. Available: <https://papers.nips.cc/paper/1991/file/8eefcfdf5990e441f0fb6f3fad709e21-Paper.pdf>
- [43] S. Ioffe and C. Szegedy, “Batch normalization: Accelerating deep network training by reducing internal covariate shift,” in *International Conference on Machine Learning*. PMLR, 2015, pp. 448–456. [Online]. Available: <https://arxiv.org/abs/1502.03167>
- [44] B. Krawczyk, “Learning from imbalanced data: open challenges and future directions,” *Progress in Artificial Intelligence*, vol. 5, no. 4, pp. 221–232, 2016. [Online]. Available: <https://journalofbigdata.springeropen.com/articles/10.1186/s40537-019-0192-5>
- [45] Y. Cui, M. Jia, T.-Y. Lin, and Y. Song, “Class-balanced loss based on effective number of samples,” in *Proceedings of the IEEE/CVF Conference on Computer Vision and Pattern Recognition*, 2019, pp. 9268–9277. [Online]. Available: [https://openaccess.thecvf.com/content\\_CVPR\\_2019/papers/Cui\\_Class-Balanced\\_Loss\\_Based\\_on\\_Effective\\_Number\\_of\\_Samples\\_CVPR\\_2019\\_paper.pdf](https://openaccess.thecvf.com/content_CVPR_2019/papers/Cui_Class-Balanced_Loss_Based_on_Effective_Number_of_Samples_CVPR_2019_paper.pdf)
- [46] N. S. Keskar, D. Mudigere, J. Nocedal, M. Smelyanskiy, and P. Tang, “On large-batch training for deep learning: Generalization gap and sharp minima,” *arXiv preprint arXiv:1609.04836*, 2016. [Online]. Available: <https://arxiv.org/abs/1609.04836>
- [47] D. Masters and C. Luschi, “Revisiting small batch training for deep neural networks,” *arXiv preprint arXiv:1804.07612*, 2018. [Online]. Available: <https://arxiv.org/abs/1804.07612>

- [48] A. S. Pearline, V. S. Kumar, S. Harini, S. M. Thampi, and E.-S. M. El-Alfy, "A study on plant recognition using conventional image processing and deep learning approaches," *Journal of Intelligent & Fuzzy Systems*, vol. 36, no. 3, pp. 1997–2004, 2019.
- [49] J. Zhang, X. Zhao, Z. Chen, and Z. Lu, "Bird species classification from an image using vgg-16 network," *Concurrency and Computation: Practice and Experience*, vol. 31, no. 23, p. e5166, 2019.
- [50] K. S. M.E., A. D. K. M.E., S. P, and S. Senthilvelan, "Birds species identification using deep learning model," in *2024 International Conference on Advances in Data Engineering and Intelligent Computing Systems (ADICS)*, 2024, pp. 1–7.
- [51] A. Dosovitskiy, L. Beyer, A. Kolesnikov, D. Weissenborn, X. Zhai, T. Unterthiner, M. Dehghani, M. Minderer, G. Heigold, S. Gelly, J. Uszkoreit, and N. Houlsby, "An image is worth 16x16 words: Transformers for image recognition at scale," 2021. [Online]. Available: <https://arxiv.org/abs/2010.11929>
- [52] H. Touvron, M. Cord, M. Douze, F. Massa, A. Sablayrolles, and H. Jégou, "Training data-efficient image transformers distillation through attention," 2021. [Online]. Available: <https://arxiv.org/abs/2012.12877>
- [53] C. Szegedy, V. Vanhoucke, S. Ioffe, J. Shlens, and Z. Wojna, "Rethinking the inception architecture for computer vision," 2015. [Online]. Available: <https://arxiv.org/abs/1512.00567>
- [54] P. Micikevicius, S. Narang, J. Alben, G. Diamos, E. Elsen, D. Garcia, B. Ginsburg, M. Houston, O. Kuchaiev, G. Venkatesh *et al.*, "Mixed precision training," *arXiv preprint arXiv:1710.03740*, 2018. [Online]. Available: <https://arxiv.org/abs/1710.03740>
- [55] B. Zhou, A. Khosla, A. Lapedriza, A. Oliva, and A. Torralba, "Learning deep features for discriminative localization," 2015. [Online]. Available: <https://arxiv.org/abs/1512.04150>
- [56] S. Abnar and W. Zuidema, "Quantifying attention flow in transformers," *arXiv preprint arXiv:2005.00928*, 2020. [Online]. Available: <https://arxiv.org/abs/2005.00928>
- [57] H. Chefer, S. Gur, and L. Wolf, "Generic attention-model explainability for interpreting bi-modal and encoder-decoder transformers," *arXiv preprint arXiv:2012.09838*, 2021. [Online]. Available: <https://arxiv.org/abs/2012.09838>
- [58] X. Shi, Y. Li, D. Yang, Y. Fang, L. Zhou, R. Wang, and L. Zhang, "Understanding the limitations of cnn-based absolute camera pose regression," *arXiv preprint arXiv:1810.03292*, 2018. [Online]. Available: <https://arxiv.org/pdf/1810.03292.pdf>
- [59] N. Monzón, "Image normalization," <http://dev.ipol.im/~nmonzon/Normalization.pdf>, 2017, accessed: 2025-04-29.
- [60] T. Ojala, M. Pietikainen, and T. Maenpaa, "Multiresolution gray-scale and rotation invariant texture classification with local binary patterns," *IEEE Transactions on Pattern Analysis and Machine Intelligence*, vol. 24, no. 7, pp. 971–987, 2002.